Coherent Flow Structures and Suspension Events over Low-angle Dunes: Fraser River, Canada

by

Ryan William Bradley

B.Sc. (Environmental Sciences), University of Guelph, 2010

Thesis Submitted in Partial Fulfillment
of the Requirements for the Degree of
Master of Science

in the
Department of Geography
Faculty of Environment

SIMON FRASER UNIVERSITY

Summer 2012

Approval

Name: **Ryan William Bradley**

Degree: **Master of Science (Geography)**

Title of Thesis: ***Coherent Flow Structures and Suspension Events over Low-angle Dunes: Fraser River, Canada***

Examining Committee:

Chair: **Dr. Eugene McCann**
Associate Professor
Department of Geography
Simon Fraser University

Dr. Jeremy Venditti
Senior Supervisor
Associate Professor
Department of Geography
Simon Fraser University

Dr. Raymond Kostaschuk
Supervisor
Adjunct Professor
Department of Geography
Simon Fraser University

Dr. Bernard Bauer
External Examiner
Professor
Earth and Environmental Sciences/Geography
University of British Columbia (Okanagan)

Date Defended/Approved: August 22, 2012

Partial Copyright Licence

Abstract

It is increasingly obvious that dunes with low-angle lee-sides (< 30°) are the most common bedform morphology in large sand-bedded alluvial channels. Flume studies have revealed much about flow and sediment dynamics over high-angle (~30°) dunes, however little is known about low-angle dunes. This study examines flow and suspension events over low-angle dunes in unsteady flow of the Fraser Estuary, Canada. Dune field bathymetry was mapped using a multibeam echo sounder while an acoustic Doppler current profiler simultaneously provided flow and suspended sediment measurements over a range of flows through tidal cycles. Mean flow and sediment transport varied through the tidal cycles. River flow dominated at low tide and large-scale suspended sediment events emerged as important sediment transport agents. I estimate that 69% of the total sediment is carried by 50% of the flow during low tide suspension events dominate the flow field.

Keywords: Fraser River; low-angle dunes; sand-bedded rivers; sediment suspension events; variable flow

To my Grandma. Thanks for all the lessons,
both big and small, about life.

Acknowledgements

I would like to thank my senior supervision, Dr. Jeremy Venditti, for seeing my potential and the continued encouragement. The freedom I had to work with my ideas was very much appreciated. I would also like to thank Dr. Ray Kostaschuk for thoughtful dune-related discussions. I would not have gotten here without your enthusiasm.

I would also like to thank Dr. Michael Church for insight about this work and rivers in general. Dr. Mead Allison and Dan Duncan for piloting our vessel and patiently answering all my multi-beam related emails. Megan Hendershot for help with field work and the tedious multi-beam processing. Maureen Attard for talks about how an aDcp works and how to process the data.

I would like to thank all the faculty, staff and students in the Geography Department. I would especially like to thank Sheena Spencer, Martin Lin, and Dr. Eugene McCann for their support.

I would finally like to thank my friends and family. They have always encouraged me to chase after my goals no matter where that has taken me.

Funding support for this work came through an Alexander Graham Bell Canada Graduate Scholarship from the Natural Sciences and Engineering Research Council of Canada (NSERC) and NSERC Discovery Grants to Venditti, Kostaschuk and Church.

Table of Contents

List of Tables

List of Figures

List of Notations

A	intercept of regression analysis
A_i	cell area
a_l	lee-side angle
a_s	stoss-side angle
a_s	sediment attenuation coefficient
a_w	water absorption coefficient
B	slope of regression analysis
C_i	suspended sediment concentration within a cell
d	depth
$<d>$	spatially averaged flow depth
D_{50}	median grain size
EI	echo intensity
f	frequency of the acoustic Doppler current profiler (aDcp)
h_i	cell height
H	dune height
H/L	dune steepness
l_i	cell length
L	dune length
L_{lee}	dune lee length
L_{stoss}	dune stoss length
L_{symm}	dune symmetry
MB	measured backscatter
n	number of at-a-point measurements

Q	quadrant number
R	distance along the aDcp beam to each cell
sf	beam-specific echo intensity scale factor
SCC	suspended silt and clay concentration
SSC	suspended sediment concentration
<SSC>	spatially averaged suspended sediment concentration
<SSC'>	deviation from the mean suspended sediment concentration
SSSC	suspended sand concentration
SWCB	sediment water-corrected backscatter
T	water temperature
<u>	mean spatial downstream velocity
<u'>	deviation from the mean spatial downstream velocity
v_{bed}	apparent bed velocity
v_{BT}	vessel velocity referenced by the bottom tracking
v_{DGPS}	vessel velocity referenced by the differential global positioning system (DGPS) unit
V	sediment volume in suspension
V_T	total sediment volume in suspension
w_i	cell width
<w>	mean spatial vertical velocity
<w'>	deviation from the mean spatial vertical velocity
WCB	water-corrected backscatter
x	subscript denoting streamwise plane
y	subscript denoting vertical plane
xy	subscript denoting both streamwise and vertical plane

Executive Summary

Dunes with low-angle lee-sides (< 30°) and symmetrical shapes are the most common bedform morphology in large sand-bedded alluvial channels. Flume studies have revealed much about the flow and sediment dynamics over high-angle (~30°) asymmetric dunes, however much less is known about low-angle dune dynamics. This study examines mean flow and suspension events over low-angle dunes in the unsteady flow of the Fraser Estuary, Canada. Dune field topography was mapped using a multibeam echo sounder (MBES) while an acoustic Doppler current profiler (aDcp) simultaneously provided flow and suspended sediment measurements over a range of tidal-influenced cycles. At high tide, river flow nearly ceases and a salt wedge enters the channel forcing plumes of salt water towards the surface into the downstream moving fresh water above. The salt wedge persists in the channel causing stratification in water column and instabilities, interpreted as one-sided Holmboe instabilities, along the saline-fresh water interface until the late in the falling tide. At low tide, mean velocities peak and force the saline water out of the channel. Flow over the low-angle dunes displays similar topographical induced patterns previously observed over high-angle dunes but permanent flow separation is not observed. Large-scale sediment suspension events dominated sediment flux during low tide but became more coherent, yet less frequent, as the tide begins to rise. Persistent and intense downwelling observed at dune crests may experience periodic sweeps that provide a mechanism for sediment erosion while a zone of persistent intense upwelling observed at the lower stoss could experience periodic ejection motions that move the eroded bed material through suspension. Suspension events are estimated to move ~69% of the total sediment in the flow above dunes when they are present in the water column.

1. Introduction

Dunes are large-scale, flow-transverse bedforms commonly found in sand-bedded channels. Dune influence on flow and sediment dynamics is controlled by dune geometry and whether the bedform is angle-of-repose asymmetric or low-angle symmetric (Kostaschuk and Villard, 1996; 1999; Best and Kostaschuk, 2002). Asymmetric dunes with long, gently sloping (2-6°) upstream stoss sides and short angle-of-repose (~30°) lee sides have been the traditional focus of research because they are easily produced in laboratories. However, a growing number of field observations has shown that symmetrical dunes with similar stoss and lee lengths and smaller lee-side angles (< 30°) are more frequent in large rivers and estuaries (Smith and McLean, 1977; Kostaschuk and Villard, 1996; Roden, 1998). Improved understanding of how such low-angle dunes interact with the flow is crucial to improve prediction of sediment transport and flow resistance in large sand-bedded rivers and estuaries.

Observations of the fluid dynamics over low-angle dunes are limited to a few studies under steady flow conditions (e.g. Smith and McLean, 1977; Kostaschuk and Villard, 1996; Best and Kostaschuk, 2002; Shugar et al., 2010). These studies have revealed mean flow patterns similar to those well documented over high-angle dunes (e.g. Nelson et al., 1993; McLean et al., 1994; Bennett and Best, 1995; Kostaschuk, 2000; Venditti and Bennett, 2000; Best, 2005a; Venditti and Bauer, 2005). Topographical fluid forcing causes a zone of maximum horizontal (downstream) velocity and positive vertical velocity as flow converges and accelerates over the crest and a

region of decelerating downward flow past the crest and into the trough. Over high-angle dunes, permanent flow separation begins at the dune brinkpoint and extends downstream to the point of reattachment. A counter-rotating eddy forms along the bottom of the trough in this separation zone. Permanent flow reversal over low-angle dunes is notably absent in field measurements (Kostaschuk and Villard, 1996), although this may be due to the limitations of the observational methodology. Indeed, a laboratory study by Best and Kostaschuk (2002) showed that the separation zone is replaced by a decelerated flow region that may experience highly intermittent near-bed flow reversal in the immediate lee region.

There have been some limited observations of flow over low-angle dunes in unsteady flow. Kostaschuk and Best (2005) observed high suspended sediment transport as flows approached maximum velocity near low tide, and suggested that increased turbulence was responsible for moving the available fine sediment deposited during low velocities at high tide. During maximum downstream flow, large-scale turbulence was observed on the surface as 'boils'. They also suggested that turbulence was enhanced as velocity initially slowed on the rising tide but decreased as flows continued to decelerate. However, the focus of Kostaschuk and Best (2005) was on dune morphological response to tidal variations and much of their discussion of the flow and sediment suspended transport was speculative.

Flow over dunes is dominated by large-scale, macroturbulent coherent flow structures that upwell through the water column where they may emerge at the surface as boils (Jackson, 1976; Babakaiff and Hickin, 1989; Kostaschuk and Church, 1993). Matthes (1947) originally referred to these structures as 'kolks' with the potential to lift and move large volumes of bed material. Indeed, there is a long series of investigations

that qualitatively suggest that these macroturbulent structures dominate sediment transport in the channel (Kostaschuk and Church, 1993; Kostaschuk and Villard, 1999; Venditti and Bennett, 2000; Best, 2005a; Shugar et al., 2010).

The form of macroturbulent structures over dunes has been described as slow rotating, upward-tilting streamwise vortices (Matthes, 1947), circular in shape with internal upwelling in the center with sharp boundaries marked by vortices (Coleman, 1969; Jackson, 1976) and ejection events (Kostaschuk and Church, 1993; Bennett and Best, 1995). Babakaiff and Hickin (1996) suggested that upwelling surface boils may appear as 'roller structures' that have an axis of rotation in the downstream-spanwise direction with ends that loop towards the center of the feature as 'horns'. Flume observations (Nezu and Nakagawa, 1993, Müller and Gyr, 1986) and observations of boils by Best (2005b) support the idea of a roller morphology, however, these authors suggest that they appear as vortex loops that have legs with a vertical-spanwise axis of rotation in addition to a rotating head. This topology is entirely consistent with the large-eddy simulation by Omidyeganeh and Piomelli (2011) who show loop vortex evolution, growth, upwelling and emergence over a dune.

The origin of these structures is not well understood, nor is their effect on sediment transport. It was originally proposed that macroturbulence is generated by near-bed boundary layer bursting processes (c.f. Kim et al, 1971; Rao et al, 1971). Jackson (1976) showed that the periodicity of 'burst' events within the turbulent boundary layer is similar to the periodicity of macroturbulent events over dunes. However, it was not clear how micro-scale boundary layer burst could grow up towards the water surface as larger structures. More recent work by Adrian (2007) has shown that small-scale hairpin turbulence can grow by the autogeneration of hairpin vortices.

He showed that small-scale hairpin vortices that form over a flat boundary at low Reynolds numbers in the near-bed logarithmic layer can occur singly or in packets. These hairpins spawn multiple streamwise-organized hairpins that organize into much larger structures that lift up into the flow. Adrian (2007) has also shown that these structures form distinct boundary layer bulges that have been observed in both the lab and at field scale.

Another oft cited initiation mechanism for macroturbulence is by K-H instabilities formed along a sharp shear layer that shed up into the flow (c.f. Kostaschuk and Church, 1993; Bennett and Best, 1995; Venditti and Bennett, 2000). Kostaschuk and Church (1993) and later work (Venditti and Bauer, 2005; Shugar, 2010) showed these vortices have a Strouhal number (frequency normalized by a length scale and velocity) consistent with eddy shedding. Many authors have argued that strong shear gradients can produce vortices that shed and amalgamate after the dune crest (Müller and Gyr, 1986; Bennett and Best, 1995; Venditti and Bennett, 2000) or grow and coalesce as they move along the shear layer towards reattachment (Nezu and Nakagawa, 1993). Nezu and Nakagawa (1993) suggested that ejection motions from the recirculation bubble accompany these processes and the intermittent shedding of these instabilities produces high instantaneous shear stress at the point of re-attachment that entrains and suspends sediment towards the surface. In the large-eddy simulation of Omidyeganeh and Piomelli (2011), the initial vortex is formed by a K-H instability suggesting that the loop vortex and instability mechanism are entirely consistent with each other.

However, the instability hypothesis for macroturbulence generation is critically depended on the presence of strong flow separation, which is absent over low-angle dunes. Best and Kostaschuk (2002) suggest that intermittent separation and flow

reversal could develop K-H instabilities that produce low magnitude and intermittent eddy generation while flow separation occurs. They also argue that a shear layer may develop even without intermittent flow separation due to the sharp velocity gradient that forms as flow decelerates over the bedform lee, producing K-H instabilities that lead to larger scale turbulence. But, observations suitable to test whether these interfaces over low-angle dunes could produce such instabilities have not be produced. This leaves open the possibility that macroturbulence is initiated via the autogeneration mechanism described by Adrian (2007).

Regardless of the generation mechanism, macroturbulent structures affect suspended sediment transport by carrying bed material from the boundary vertically in the flow. Rood and Hickin (1989), for example, used surface grabs of suspended sediment from surface boils and showed that boils had higher sediment concentrations and larger grain sizes than the ambient flow. A flume study by Venditti and Bennett (2000) and field observations by Kostaschuk (2000) over high-angle dunes suggest that coherent flow structures are responsible for advecting bed material up into the downstream flow. Recently, Shugar et al. (2010) showed that macroturbulent structures suspend sand from the bed as 'ejections' into the flow over a dune with a lower lee angle (21.8°). Structures were observed to grow with height above the bed and break up as they were advected downstream, releasing the sand.

In spite of these insights into flow and sediment transport over low-angle dunes, three critical questions remain about the coupling between unsteady flow and low-angle dune topography: 1) How does the mean flow structure change over low-angle dunes in unsteady flow?; 2) What are the characteristics of suspension events and how do the events evolve over low-angle dunes? and 3) What is the linkage between sediment

suspension and flow over low-angle dunes? Recent advances in field instrumentation provide opportunities for high-resolution spatial and temporal measurements that allow for detailed investigations of these questions. I use multibeam echosounding and simultaneous acoustic Doppler current profiler transects to explore flow over low-angle dunes through semidiurnal tidal cycles in the Main Channel of the Fraser River estuary, British Columbia, Canada. The analysis focuses on the mean flow structure and sediment suspension events, and how these change with tides.

2. Methods

2.1. Study area

Field measurements were collected in the Main Arm of the Fraser River near Steveston, British Columbia, Canada (Figure 1). The Fraser River discharges into the Strait of Georgia on the west coast of Canada, draining 234 000 km² of mountainous terrain. Mean annual river discharge at Mission (40 km upstream) is 3 410 m³/s with a mean annual flood of 9790 m³/s (McLean et al., 1999). Approximately 80% of the annual total discharge occurs during the spring snow-melt freshet between May and July (Villard and Church, 2003). The lower reach of the river, near Steveston, is affected by mixed semi-diurnal tides with daily inequalities in the heights of two high and low tides. At the mouth of the river, the mean tidal range is 3.1 m with extreme spring tides of over 5.4 m (Villard and Church, 2003). This estuarine reach of the Fraser River experiences a salinity intrusion that migrates upstream into the channel during rising tides and is forced downstream during falling tides. Median grain size in the estuary is 0.25 to 0.32 mm with little seasonal and spatial variation (Kostaschuk et al., 1989). Nine bed-material samples that were collected using a grab sampler on 17 June 2010 and later sieved revealed a D_{50} of 0.27 mm. Bed-material grain-size distributions are provided in Figure *2*.

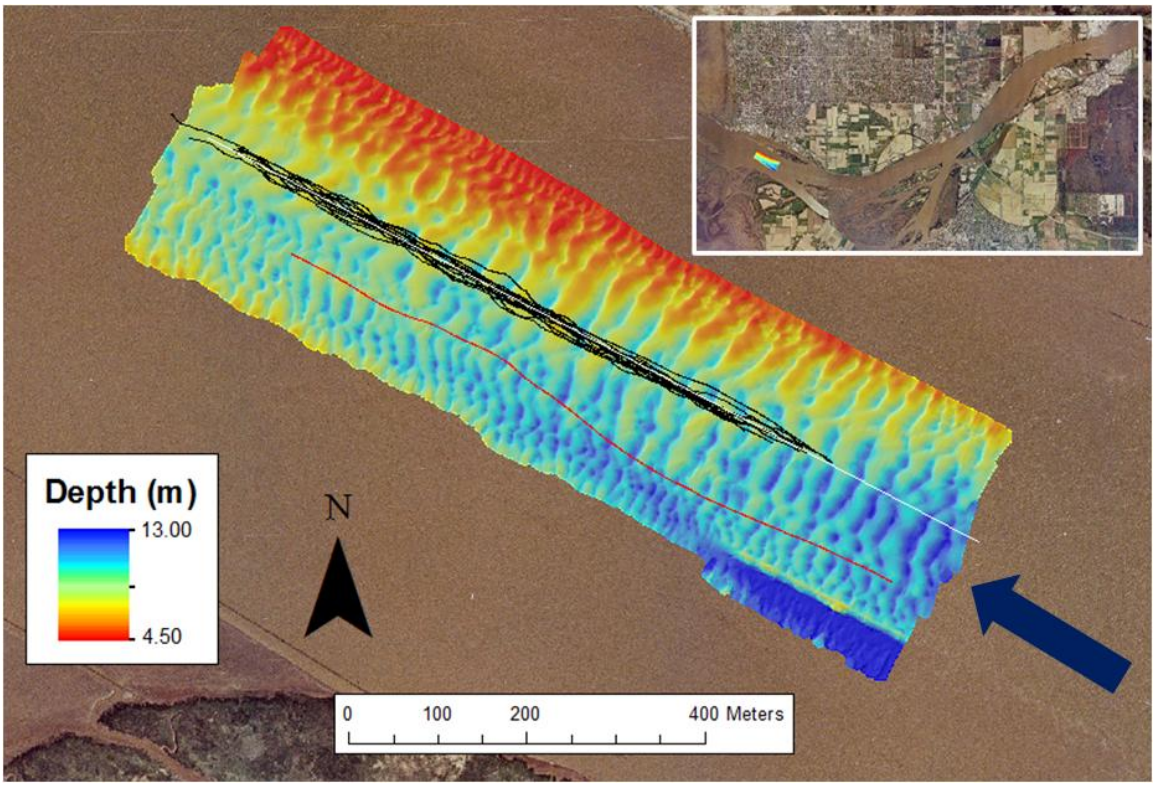

Figure 1. Bathymetric contour map of the study dune field (Survey G). Inset shows the position of the dune field in the Main Arm of the Fraser River, British Columbia. Black lines show the downstream travelling aDcp lines and the red line shows the upstream aDcp line (K2). The white line indicates the transect used to quantify dune morphology and the blue arrow indicates flow direction.

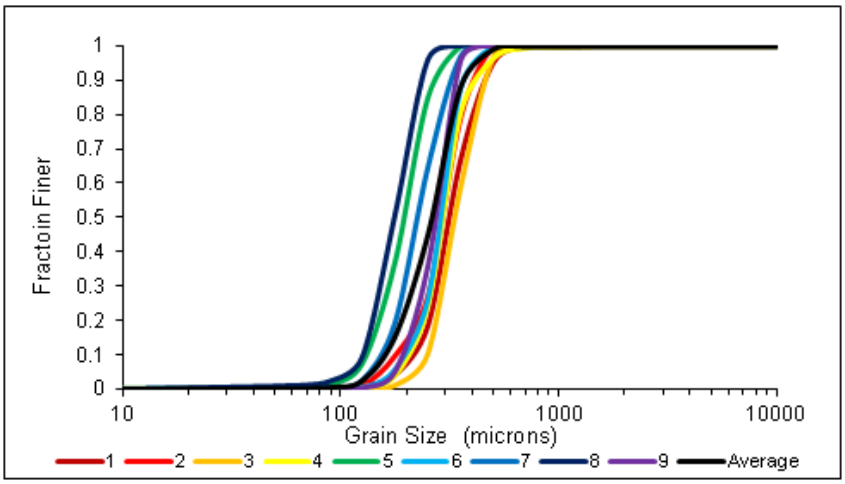

Figure 2. Bed material grain-size distribution for each sample and the average of the 9 sample.

2.2. Data collection

Three-dimensional (3D) bathymetry and 3D flow velocities were measured from the R/V *Lake Itasca* between 12 and 17 June 2010. Bathymetry was measured using a Reson 7101 Seabat Multibeam echo-sounder (MBES) while 3D flow velocities were simultaneously recorded using a Teledyne RD Instruments 1200 kHz Rio Grande Workhorse acoustic Doppler current profiler (aDcp). The MBES positioning was measured using a Real Time Kinematic GPS accurate to 0.01 m horizontally and 0.02 m vertically. The position of the aDcp was recorded using a GPS differentially corrected by a Canadian Coast Guard beacon about 1.70 km south of the dune field. The differential GPS provides positioning with an accuracy of 0.25 m horizontally and 0.50 m in the vertical.

The Reson 7101 Seabat Multibeam operates at 240 kHz to provide detailed bathymetry at a manufacturer reported depth resolution of 1.25 cm (Reson Inc., 2009). A projector array on the sonar head transmits fan-shaped pulses or 'pings' of acoustic energy into the water column and reflections from the bed are captured on a receiver array on the sonar head. The bottom is detected using a combination of centre-of-energy, phase-zero crossing algorithms and blended amplitude and phase detection methods (Reson Inc., 2009). The head generates 511 equidistant beams and measures relative water depths over a 150° wide swath perpendicular to the vessel track. Navigation, orientation, and attitude data (heave, pitch, roll) were recorded using an Applanix POS MV V3 gyroscope inertial guidance system mounted inside the vessel hull.

Three-dimensional flow velocities were measured at a vertical resolution of 0.25 m (vertical bin size) with the aDcp. The RD Instruments aDcp has a 4 beam and

transducer system that emits and receives acoustic ‘pings’ of energy. The transmitted acoustic pulses are backscattered by particles that are assumed to be moving at the same velocity as the water. The sound reflected back is Doppler-shifted to a lower frequency proportional to the relative velocity between the aDcp and particles in the water column. The change in frequency is then converted into weighted averages of the components of flow velocity within each bin (Teledyne RD Instruments, 2001). Velocity is calculated relative to the instrument head thus measured velocities must be corrected by removing the vessel velocity as determined by bottom track or the GPS. Bottom tracking measures the Doppler shift in frequency with respect to the bed. The aDcp provides velocity measurements with a manufacturer reported accuracy of $\pm$ 0.5 cm/s and echo intensity with a precision of $\pm$ 1.5 dB (Teledyne RD Instruments, 2001). The aDcp was set to ping at 11 Hz and pings were averaged in ensembles every 0.45 seconds to improve the signal to noise ratio providing velocity measurements at approximately 2.2 Hz. Average vessel velocity over the transects was about 1.54 m/s, resulting in profiles every 0.71 m. Averaging in the water column occurs over different volumes of water because each beam is oriented at an orthogonal angle of 20° in the vertical and beam spreading occurs at 1.5°.

MBES and aDcp measurements of a dune field approximately 1 km long and 0.5 km wide were made over multiple tidal cycles with the intent of capturing a range of flow conditions (Figure 1). Figure 3 shows river stage at Steveston and daily mean discharge at Mission (~40 km upstream of study area) for the measurement period. Bed elevation and flow velocity measurements were made during 14 surveys over a 4 day period. Individual surveys were grouped into ‘Upper Falling Tide’, ‘Lower Falling Tide’, ‘Low Tide’, ‘Lower Rising Tide’, ‘Upper Rising Tide’ and ‘High Tide’ according to their location within individual cycles in order to allow cross cycle comparisons (Figure 3). Each survey

consisted of 5 parallel streamwise transects that produced a continuous, overlapping bed map and 5 streamwise velocity transects.

ADcp results reported herein are from the centremost transects over the most well-defined dunes measured while the vessel was travelling upstream (Figure 1). Transects were measured with the boat moving in both the upstream and downstream direction but only the centremost upstream transects were included in the analysis because the flow is observed in a moving Eulerian framework. This framework provides a nearly instantaneous view of large sediment suspension events as they pass beneath the vessel and the spatial flow structure over the dunes as the boat moves over the bed. Downstream transects were generally captured as the boat moved faster than the surface flow in order to maintain vessel control during high downstream velocities at lower tide stages. This obscured observations of suspension events and the mean flow structure by stretching them in the downstream direction to varying degrees depending on vessel velocity. Nevertheless, the observations are similar regardless of which direction the boat was moving. During the High Tide Survey K, aDcp results are reported from a transect (K2) that is south of the centerline while the boat was travelling upstream (Figure 1). Flow was dominantly upstream during this survey so observations are still in a semi-Eulerian framework.

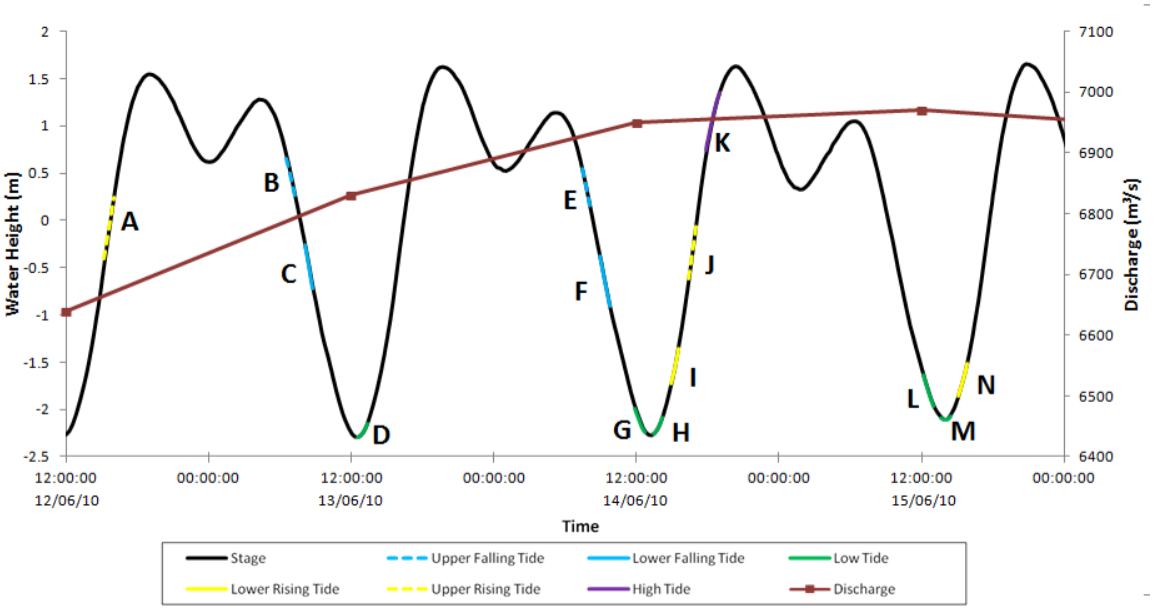

Figure 3. River stage (corrected to Geodetic Survey of Canada datum) at Steveston and discharge at Mission (40 km upstream of study reach) for sampling period. Survey periods are marked by letters A-N. Five-minute averaged river stage data for Water Survey of Canada (WSC) station 08MH028 provided by Lynne Campo (by request) and discharge data from WSC station 08MH024 available online at <http://www.wsc.ec.gc.ca/applications/H2O/graph-eng.cfm?station=08MH024&report=daily&year=2010> accessed 2 August 2012.

Suspended sediment samples were collected on 17 June 2010 to calibrate aDcp backscatter to suspended sediment concentrations. A USGS P-63 point-integrating suspended sediment sampler was opened for 40 seconds at each of 0.1d, 0.2d, 0.4d, 0.6d and 0.8d (where d = depth) to measure sediment concentrations. Three profiles were measured; one during Low Tide, one during Lower Rising Tide and one at the Upper Rising Tide stage. Grain size distribution of the samples was measured using a Sequoia LISST-Portable that uses laser diffraction to provide grain size distribution within a range of 1.9-381 µm. Filtration using 47 mm microfibre filters with pore size of 1.6 µm, was used to obtain sediment concentrations.

2.3. MBES and aDcp processing

Raw MBES data were imported into CARIS HIPS® software for postprocessing where lines and soundings were merged to produce bathymetric grids. This software allows for the removal of 'bad pings' and corrections for changes in heave, pitch and roll and tidal stage. The data were then imported into ArcGIS® and gridded at 1 m for further analysis of the bed surface and measurements of bedform characteristics. The processed bed surface maps were used to obtain bed profiles along aDcp transects because it provides a more accurate view of the bed. A streamwise transect that corresponded to the analyzed downstream-travelling aDcp transects was drawn through the bedform field of Survey G (Figure 1) to obtain all bedform measurements.

A software package developed by Colin Rennie (University of Ottawa) (eg. Rennie and Rainville, 2006; Rennie et al., 2007; Rennie and Church, 2010) was used to extract the aDcp data and correct for the magnetic variation, depth of the transducer below the surface, and height of the GPS receiver above the instrument. The software also allows correction of measured velocities by removing the vessel velocity referenced by the DGPS (v_{DGPS}) or bottom tracking (v_{BT}). Bottom track should be limited to immobile bed conditions as a mobile bed produces bias in the measured frequency of the Doppler shift because the shift is related to both the boat and bed velocities. This bias allows for an estimate of apparent bed velocity (v_{bed}) as (Rennie et al. 2002):

$$v_{bed} = v_{DGPS} - v_{BT} \quad (1)$$

I chose to use bottom tracking when the estimated bed velocity was near the range of the instrument error because some of the velocity data experienced 'gaps' when the DGPS was used as a reference. Transects included in this analysis that used

the DGPS as a reference did not experience DGPS failure and thus were not contaminated. Table 1 reports the estimated bed velocity for each transect as well as the reference used to calculate velocities.

Table 1. Estimated bed velocity data, references for velocity corrections and the availability of vertical velocity data.

Position in Tidal Cycle	Transect	Transect Time (s)	GPS Transect Length (m)	BT Transect Length (m)	v_{bed} (m/s)	Reference Used	Vertical Velocity*
Upper Falling	B	626	1024.7	1021.4	-0.005	BT	N
	E	556	981.7	969.3	-0.022	BT	N
Lower Falling	C	636	1011.1	985.3	-0.041	BT	N
	F	680	996.2	969.9	-0.039	BT	N
Low	L	839	994.5	1696.2	0.836	GPS	Y
	G	960	1017.3	2056.8	1.083	GPS	Y
	M	869	994.4	1801.0	0.928	GPS	Y
	D	795	1013.6	1751.8	0.928	GPS	Y
	H	787	977.3	1613.6	0.808	GPS	Y
Lower Rising	N	589	973.6	1173.6	0.340	GPS	Y
	I	461	976.6	1073.0	0.209	GPS	Y
Upper Rising	J	437	945.4	945.1	-0.001	BT	Y
	A	416	929.0	930.6	0.004	BT	Y
High	K	763	947.5	945.0	-0.003	BT	Y
	K2	578	984.6	995.0	0.018	BT	Y

*Refers to the availability of vertical velocity data without contamination. See Figure 4 for further explanation.

Velocity records were also periodically and variably affected by large surface waves that caused ‘up and down’ vertical vessel motion. Figure 4 shows an example from Transect E with particularly strong influence of vertical vessel motion on reported vertical velocities. Apparent vertical velocity reported along a horizontal plane near the surface should show limited variation, however, the vertical velocity fluctuates in an ‘up and down’ motion that roughly corresponds to the changes in vessel altitude as recorded by the DGPS (Figure 4a). This issue resulted in contaminated vertical flow field maps (Figure 4b) for some of the surveys. Attempts to remove the altitude signal from the vertical velocity records by taking the derivative of the altitude signal in the time domain and correcting for lags between the signals were unsuccessful because the lags were

inconsistent and vertical velocity response to altitude changes varied in strength. As a result, there were no useful vertical velocity measurements during the Upper Falling and Lower Falling transects (Table 1) and so they were not included in the analysis. The remaining transects showed minimal contamination from the changes in altitude of the boat and thus were included in this analysis. Nonetheless, care must be taken when interpreting vertical velocities recorded from an aDcp on a moving vessel.

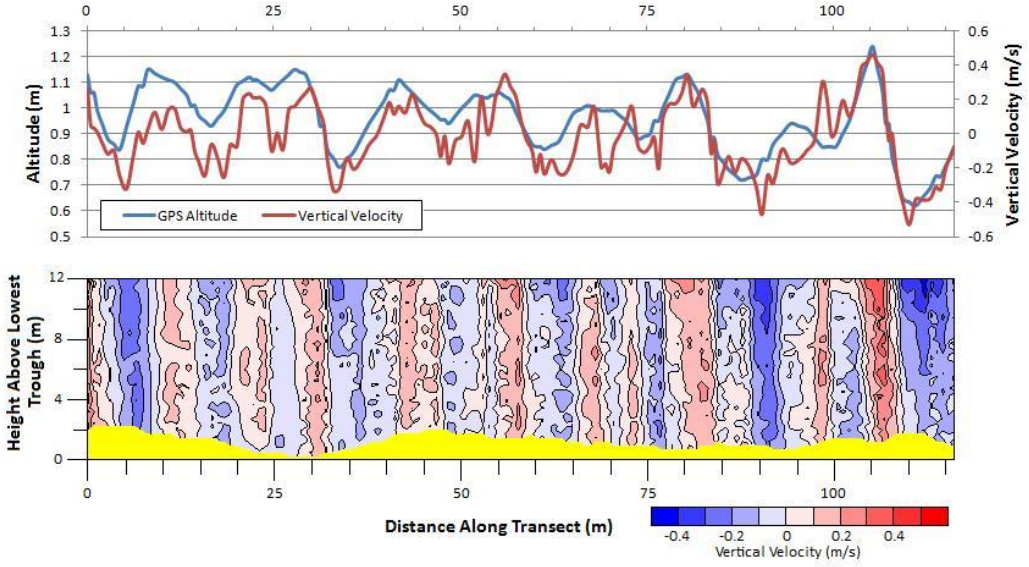

Figure 4. a) The influence of altitude change on vertical velocity measurements along an equidistant row across the top of the profiles. b) Contour map of the vertical velocity flow field showing contamination from altitude change.

2.4. Calibration of aDcp backscatter to suspended sediment concentrations

Echo Intensity (EI) recorded in counts or backscatter strength of an aDcp acoustic return can be used to estimate the concentration of suspended sediment in a wide range of flows (Kostaschuk et al., 2005; Topping et al., 2007; Domarad, 2010). Backscatter strength is a function of sediment particle size, type and concentration, thus, backscatter is directly proportional to concentration for a constant sediment type and

size (Kostaschuk et al., 2005). In this study, EI was converted to total suspended sediment concentration using the calibration methodology developed by Topping et al. (2007) and Wright et al. (2010) that applies underwater acoustic theory to correct for both water and sediment absorption. This first step in this calibration is to convert the EI recorded by the aDcp into measured backscatter MB:

$$\mathrm{MB} = \mathrm{sf} * \mathrm{EI} \quad (2)$$

where sf is a beam-specific echo intensity scale factor obtained from RD Instruments. The forward facing beam was selected for this analysis and has an instrument specific sf = 0.383 dB/count. Changes in backscatter through the water column may be caused by water absorption and beam spreading thus, water-corrected backscatter (WCB) is calculated as:

$$\mathrm{WCB} = \mathrm{MB} + 20\log_{10}\mathrm{R} + 2\mathrm{a_w}\mathrm{R} \quad (3)$$

where R is the distance along the beam to each cell and $\mathrm{a_w}$ is the water absorption coefficient. Assuming zero salinity, $\mathrm{a_w}$ is calculated (Schulkin and Marsh, 1962) as:

$$\mathrm{a_w} = 8.686 * 3.38\mathrm{x}10^{-6}\frac{\mathrm{f}^2}{\mathrm{f_T}}, \quad (4)$$

$$\mathrm{f_T} = 21.9\mathrm{x}10^{\left[6-\frac{1520}{\mathrm{T}+273}\right]} \quad (5)$$

where f is the frequency of the aDcp and T is the water temperature in ^{o}C. Suspended sediment concentration (SSC) is calculated from the sonar equation for sound scattering from small particles (Gartner, 2004):

$$\log(\mathrm{SSC}) = \mathrm{A} + \mathrm{B} * \mathrm{WCB} \quad (6)$$

where A and B are the intercept and slope from a regression of calculated WCB and physically collected suspended sediment concentrations. Water-corrected backscatter WCB values from the same depth as the P-63 samples were selected and plotted on a semi-log scale to correlate with total suspended sediment concentration measured from the P-63 (Figure 5a). Water-corrected backscatter (WCB) explains 86% of the variability in total SSC suggesting that it is a good means of estimating total suspended sediment.

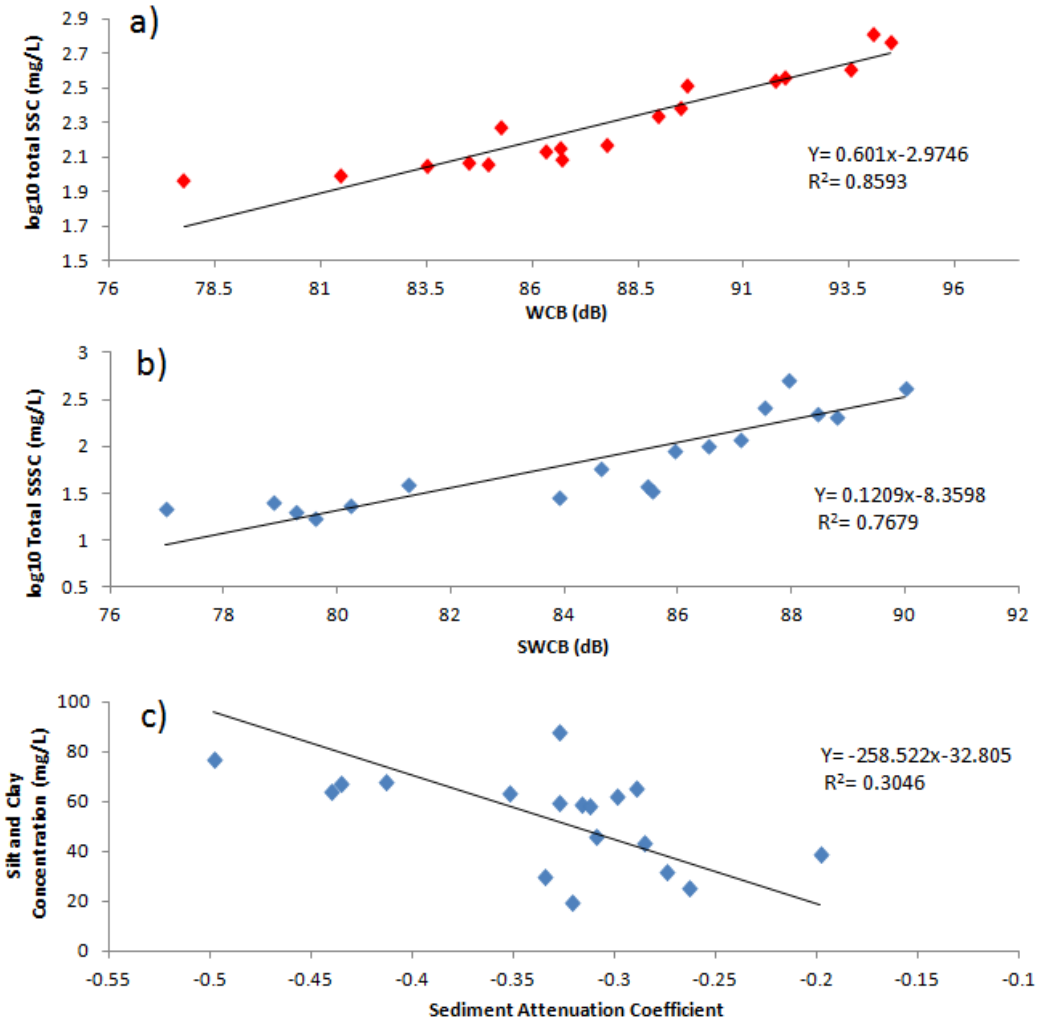

Figure 5. a) Calibration curve of Total Suspended Sediment (SSC) with Water-corrected Backscatter (WCB). b) Calibration curve of Total Suspended Sand Concentration (SSSC) with Sediment Water-corrected Backscatter (SWCB). c) Calibration curve of Total Silt and Clay Concentration with Sediment Attenuation Coefficient (a_s). All fitted lines have been corrected using the reduced major axis correction (see Mark and Church, 1977) because they are formal calibrations.

Topping et al. (2007) and Wright et al. (2010) extend their method to discriminate silt and clay from suspended sand concentrations (SSSC) using:

$$\mathrm{SSSC} = 10^{(\mathrm{A}+\mathrm{B}*\mathrm{SWCB})} \qquad (7)$$

where SWCB is sediment water-corrected backscatter. Sediment water-corrected backscatter SWCB corrects for two-way sediment attenuation losses in addition to water absorption:

$$\mathrm{SWCB} = \mathrm{WCB} + 2a_s R \tag{8}$$

where a_s is the sediment attenuation coefficient computed as:

$$a_s = -\frac{1}{2}\overline{\frac{d}{dR}(\mathrm{WCB})} \tag{9}$$

where $\overline{\frac{d}{dR}(\mathrm{WCB})}$ denotes the slope of the least-squares linear regression between WCB and R.

Values of SWCB calculated at the sample depth of the P-63 samples were selected and plotted on a semi-log scale to correlate with total sand concentration (Figure 5b). Silt and clay concentrations (SCC) were plotted on a linear scale because sediment attenuation is linearly related to SCC (Figure 5c). While the SWCB and sand concentration calibration is significant and provides a strong R^2 value, it is weaker than the calibration with total SSC and WCB (Table 2). The calibration of sediment attenuation to the measured SCC is not significant, has a smaller R^2 and is inversely correlated (Figure 5c, Table 2), suggesting size discrimination is not possible for this data. The Topping et al. (2007) and Wright et al. (2010) method was developed for a side-facing aDcp where sediment concentration does not vary along the aDcp beams. Correlation with the sediment attenuation therefore may not be appropriate when suspended sediment concentrations and grain-size increase towards the bed. In consideration of this, WCB calibration is used as (Figure 5a):

$$SSC = 10^{0.0601(WCB)-2.9746} \quad (10)$$

This calibration does not allow for discrimination between sand and clay but does provide reasonable estimates of total SSC.

Table 2. Regression results for the aDcp calibrations (Figure 5)

Calibration	Functional Regression Equation	R^2	p-value
Water-corrected backscatter	$SSC = 10^{0.0601(WCB)-2.9746}$	0.8593	<0.0001
Sediment water-corrected backscatter	$SSSC = 10^{0.1209(SWCB)-8.3598}$	0.7679	<0.0001
Sediment attenuation coefficient	$SCC = -258.522a_s - 32.805$	0.3046	0.7551

2.5. Examination of the flow structures over low-angle dunes

Two-dimensional plots of mean velocity over dunes reveal little about the spatial flow structure beyond topographically-forced acceleration over the stoss and deceleration over the lee because velocity generally increases logarithmically above the bed. A more effective method to identify spatial patterns is to 'vertically detrend' the at-a-point downstream velocity (u_{xz}) and vertical velocity (w_{xz}) measurements. This was accomplished by calculating the mean velocity along horizontal equidistant planes at 0.25 m intervals (bin spacing) from the water surface and subtracting the calculated mean from the instantaneous velocities along the plane. Mean horizontal velocity $<u>_x$ and mean vertical velocity $<w>_x$ are spatial mean flow velocities calculated for each horizontal plane in the vertical as:

$$\langle u \rangle_x = \frac{\sum_{x=1}^{n} u_{xz}}{n} \quad (11)$$

$$\langle w \rangle_x = \frac{\sum_{x=1}^{n} w_{xz}}{n} \quad (12)$$

where u_x and w_x are at-a-point horizontal and vertical velocities within the plane and n is the number of measurements. Angle brackets indicate a spatial average and the subscripts indicate the plane along which the spatial average is calculated (x for streamwise, z for vertical, xz for streamwise and vertical). The calculated $<u>_x$ and $<w>_x$ were then used to detrend u_x and w_x for each plane as:

$$u'_{xz} = u_{xz} - \langle u \rangle_x \quad (13)$$

$$w'_{xz} = w_{xz} - \langle w \rangle_x \quad (14)$$

where u'_{xz} and w'_{xz} are the deviations from $<u>_x$ and $<w>_x$ along the plane. This method of detrending was used for each horizontal plane in the vertical array of stacked planes. The resulting vertically detrended velocity contour plots allow for observations of velocity deviation from the mean flow in a semi-Eulerian framework.

These data were then used for a 'spatial quadrant analysis'. Quadrant analysis is typically used to identify turbulent events by separating at-a-point instantaneous fluctuations of downstream and vertical velocity from time-averaged mean values into quadrants (e.g.,Lu and Willmarth, 1973; Bennett and Best, 1995; Nelson et al., 1995). However, I do not have the at-a-point time series data for the traditional analysis, thus I identify persistent upwelling and downwelling patterns in the flow by separating observed velocities in each ensemble profile into quadrants 1 ($+u'_{xz}, + w'_{xz}$), 2 ($-u'_{xz}, + w'_{xz}$), 3 ($-u'_{xz}, - w'_{xz}$) and 4 ($+u'_{xz}, - w'_{xz}$) based on deviations from the spatial means. A moving average of 7 adjacent ensembles (3.15 seconds) for each velocity profile was used on the velocity measurements before detrending and separating into quadrants to reduce

noise and better identify patterns in the flow. I also applied a threshold that identified regions of particularly strong upwelling (quadrant 2) and downwelling (quadrant 4) that exceeded the spatial mean downstream and vertical velocity by at least 10% in the flow. These regions provide insight into consistent patterns of upwelling fluid that are preceded by downwelling fluid in a fashion similar to observed signatures of macroturbulence (Kostaschuk and Church, 1993; Bennett and Best 1995, Best 2005). I focus my analysis on Quadrant 2 and Quadrant 4 because they have been identified as important agents in the entrainment and transport of bed material (Bennett and Best, 1995; Venditti and Bennett, 2000).

2.6. Examination of sediment suspension over low-angle dunes

Suspended sediment patterns over dunes were highly variable so mean suspended sediment concentration $<SSC>_{xz}$ was calculated as

$$\langle \mathrm{SSC} \rangle_{xz} = \frac{\sum_{x=1}^{n_x} \sum_{z=1}^{n_y} \mathrm{SSC}_{xz}}{n} \quad (15)$$

where SSC_{xz} is at-a-point suspended sediment concentration, n_x is the number of horizontal planes, and n_y is the number of vertical planes. Deviation from the mean suspended sediment concentration $\mathrm{SSC'}_{xz}$ was calculated as:

$$\mathrm{SSC'}_{xz} = \mathrm{SSC}_{xz} - < SSC >_{xz} \quad (16)$$

$\mathrm{SSC'}_{xz}$ contour maps provide a nearly instantaneous view of suspended sediment transport patterns. It should be noted however, that SSC_{xz} cannot be separated from backscatter peaks associated with density gradients between saline and fresh water,

which limits this investigation of SSC over low-angle dunes to periods when there is no salt water in the channel, that is at Low Falling, Low and Low Rising tidal stages (Table 1).

2.7. Identification of flow structures and sediment suspension events

ADcp beam geometry and measurements from a moving vessel limit observations of turbulence in my velocity measurements. Sampling volume increases with depth because beams are oriented at 20° in the vertical and beam spreading occurs at 1.5° while the average distance of 0.71 m between ensembles adds to the sampling volume. These factors create sampling diameters of 2.23 m at 2 m below the surface, 5.26 m at 6 m and 9.80 m at 12 m (Figure 6). Coherent flow structures are required to be larger than these sampling volumes in order to appear in the velocity measurements, thus they are not obvious in most of the velocity data. However, sediment suspension events are clearly defined in the SSC'_{xz} records because I selected only the forward facing beam to reduce the sampling volume. SSC_{xz} measurements occur over much smaller sampling diameters of 0.76 m at 2 m below the water surface, 0.87 m at 6 m and 1.02 m at 12 m (Figure 6).

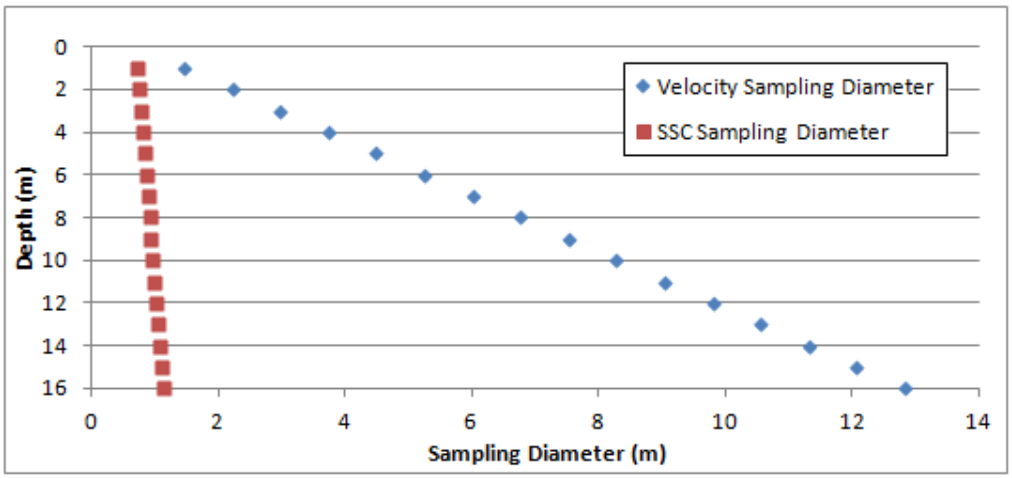

Figure 6. Comparison of velocity and suspended sediment concentration aDcp sampling diameters.

It is important to note that the spatial quadrant analysis does *not* identify ejections, sweeps, inward interactions or outward interactions typically inferred from time-series quadrant analysis (e.g. Bennett and Best, 1995). The geometry of the aDcp beams is not appropriate for time-series quadrant analysis and these data are collected from a moving vessel, thus temporal fluctuations of velocity at-a-point (turbulence) cannot be separated from spatial fluctuations from the mean.

3. Results

3.1. Dune characteristics

Dune profile geometry and three-dimensionality varied both spatially and temporally over the measurement period. Individual bedforms changed through the tidal cycles because of active dune migration during unstratified flow around low tide. The bathymetric maps (Figure 1) also reveal the presence of bar topography on the northern channel bank. Dune size generally increased in size as they moved over the bar consistent with observations by Villard and Church (2003). Because spatial and temporal changes of dunes are beyond the scope of this study, I only present dune morphological statistics from a low tide survey (G) to characterize the dunes in the study field. Summary statistics in Table 3 are from 18 well-defined dunes with heights that exceeded 0.5 m. The mean lower lee-side slope (a_l) of the dunes was 11.94°, typical of low-angle dunes in large rivers (e.g. Smith and McLean 1977; Kostaschuk and Villard, 1996; Roden, 1998), and mean symmetry L_{symm} ($L_{symm} = L_s/L_l$ where L_s and L_l are the stoss length and lee length relative to the crest) was 1.20. A perfectly symmetrical dune has $L_{symm} = 1.0$ and an asymmetric 'angle-of-repose' dune (assuming a height and length of the mean of the dunes observed here) has $L_{symm} = 14.4$. None of the bedforms displayed the lee-side 'angle-of-repose' (>30°) geometry typical of high-angle dunes. These dune characteristics were very similar to the low-angle dunes previous observed by Kostaschuk and Villard (1996) in this reach of the Fraser River.

Table 3. Morphological characteristics of dunes along transect in Survey G (Figure 1).

	Height	Length	Steepness	Symmetry*	Lee Side Slope	Stoss Side Slope
	H (m)	L (m)	H/L	L_{smm}	a_l (°)	a_s (°)
Mean	1.49	37.29	0.04	1.20	11.94	5.17
Max	2.39	51.94	0.08	2.00	21.90	9.30
Min	0.72	12.98	0.02	0.41	3.32	1.0

3.2. Mean flow, water-corrected backscatter and suspended sediment concentrations

The mean flow and suspended sediment concentrations over the dune field varied with the tidal cycle. Table 4 summarizes mean spatially-averaged suspended sediment concentration $<SSC>_{xz}$ and downstream velocity $<u>_{xz}$ calculated as:

$$\langle u \rangle_{xz} = \frac{\sum_{x=1}^{n_x} \sum_{y=1}^{n_y} u_{xz}}{n} \qquad (17)$$

As noted above, $<SSC>_{xz}$ is not reported when saline water is present in the channel (Transects B, C, E, F, and K2). Spatially averaged flow depth $<d>_x$ is the averaged flow depth (d) along the transect.

Table 4. Descriptive flow and suspended sediment statistics for each transect.

Position in Tidal Cycle	Transect	$\langle u \rangle_{xz}$ (m/s)	$\langle SSC \rangle_{xz}$* (mg/l)	$\langle d \rangle_x$ (m)
Upper Falling	B	0.89	-	13.51
	E	0.93	-	13.53
Lower Falling	C	1.45	-	12.85
	F	1.60	-	11.08
Low	L	1.95	439.87	11.45
	G	2.20	413.20	11.06
	M	2.07	408.17	11.07
	D	2.05	397.21	10.94
	H	1.97	372.75	10.89
Lower Rising	N	1.41	287.35	11.36
	I	1.23	211.31	11.53
Upper Rising	J	0.30	55.25	12.59
	A	0.14	41.78	12.79
High	K	0.13	30.58	13.99
	K2	-0.18	-	15.34

*SSC is not calculated when salinity intrusion is present in the channel because calibration assumes zero salinity

At High Tide, flow in the channel nearly stopped as $\langle u \rangle_{xz}$ reached the lowest measured point of 0.13 m/s (Transect K) with evidence of weak upstream flow (Transect K2). As the tide began to fall (Transect B and E), $\langle u \rangle_{xz}$ was about 0.9 m/s and continued to accelerate with the falling tide (Transect C and F). During Low Tide transects (L, G, M, D and H), $\langle d \rangle_x$ approached a minimum of 10.89 m and $\langle u \rangle_{xz}$ peaked at 2.2 m/s. The peak in $\langle u \rangle_{xz}$ preceded the lowest $\langle d \rangle_x$ suggesting that depth response to tidal change lagged behind velocity. As tides rose, $\langle u \rangle_{xz}$ steadily decelerated from about 1.2 m/s during the Lower Rising tide transects (N and I) to 0.2 m/s during the Upper Rising tide transects (J and A). The spatially-averaged downstream velocity was greater during the falling tide than on the rising tide.

The maximum measured $\langle SSC \rangle_{xz}$ of 439.87 mg/l occurred during the first Low Tide transect (L) suggesting that the actual peak may have occurred before the Low Tide measurement records. Maximum $\langle u \rangle_{xz}$ lagged behind the peak in $\langle SSC \rangle_{xz}$ suggesting that a large supply of finer bed material is transported out of the channel early in the tidal

fall and that less sediment was readily available for transport when $\langle u \rangle_{xz}$ peaked. The easily eroded bed-material likely represents fine sediment that settled to the bed during the near slack water a high tide. Later during the Low Tide transects (M, D, H), $\langle SSC \rangle_{xz}$ was high but began to decrease as less sediment was readily available for transport and flow velocities began to slow. Early in the Rising Tide (Transects N, I), $\langle SSC \rangle_{xz}$ continued to decrease as $\langle u \rangle_{xz}$ decreased. As tides approached maximum height, $\langle SSC \rangle_{xz}$ was relatively low.

Figure 7 shows vertical profiles of downstream velocity, WCB and SSC, averaged along lines equidistant from the water surface (eq. 11) for transects within the different stages of the tidal cycle. I show both WCB and SSC because SSC cannot be reliably calculated during periods when saline water is present in the channel and WCB reveals the nature of the saline-fresh water interface in the channel. Early in the tidal fall (Figure 7a), the salt wedge intrusion was evident in the lower portion of the profile, causing stratification in the flow. Downstream velocity $\langle u \rangle_x$ was greatest in the upper fresh water layer but sharply declined in a zone about 10 to 13 m above the bed. This sharp decline may be due to friction imposed by the slow moving saline wedge below. From 7 to 10 m above the bed, $\langle u \rangle_x$ decreased more slowly and the lower part of the profile (below 10 m) shows that velocity was constantly small, yet positive, indicating that the wedge was no longer migrating upstream and was beginning to retreat from the channel. It is difficult to identify the exact transition from the fresh to saline water in the $\langle u \rangle_x$ profile, however, the $\langle WCB \rangle_x$ reveals the transition between the two different density layers as a peak from 9.5 to 11.5 m. Sharp density gradients at the pycnocline are recorded as peaks in backscatter that can be used to visualize the position and structure of the saline-freshwater interface in the flow (Geyer and Farmer; 1989, Tedford et al., 2009, Kostaschuk et al., 2010). From the pycnocline to the water surface,

$\langle WCB_x \rangle$ steadily decreased suggesting that there is no longer a sharp density gradient and that mixing decreases away from the pycnocline towards the surface. At 9.5 m, $\langle WCB_x \rangle$ also decreased but remained constant to the near-bed region, which I interpret as a constant density with minimal mixing within the wedge.

The flow was no longer highly stratified later in the tidal fall (Figure 7b) and $\langle u \rangle_x$ decreased more gradually from the surface until about 7 m where there was a sharp kink in the profile typically observed in spatially averaged flow over dunes (McLean and Smith, 1977; McLean et al., 1994; McLean et al., 1999). This kink reveals a stronger influence of the bed as it exerts friction that retards the flow. Within the range of the bed maximum and minimum, $\langle u \rangle_x$ slowed more rapidly as topographic forcing produced flow expansion in the bedform troughs. The peak in the $\langle WCB_x \rangle$ that defined the pycnocline is no longer evident but it is likely that saline water has not been completely flushed from the channel. The value of $\langle WCB_x \rangle$ increased from the surface linearly until about 6 m where there was a weak kink in the profile, suggesting that higher SSC from bed-material resuspension was contributing to the WCB in the lower profile rather than simply saline water contributing to the backscatter.

During Low Tide (Figure 7c), when downstream velocity and suspended sediment concentrations were the largest of the cycle, the profiles shows no evidence of saline water and are typical of steady flow observations over dunes in this reach of the Fraser River (Kostaschuk and Villard, 1996). Mean downstream velocity $\langle u \rangle_x$ decreased relatively slowly from the surface until 3.5 m where there was a distinct kink in the velocity profile. This sharp decrease in $\langle u \rangle_x$ occurred within the range of the maximum and minimum bed height and illustrates the strong influence of bedform morphology on the mean downstream flow. Investigation of individual dune troughs

showed no negative downstream velocity suggesting no flow separation was present in the field, although the aDcp beam geometry makes measurements of near-bed velocity difficult. Values of $\langle SSC \rangle_x$ decreased nearly linearly above the bed, reflecting the typical decrease in turbulent sediment suspension capacity above the bed in unstratified flow (Kostaschuk and Villard, 1999; Kostaschuk, 2000; Shugar et al., 2010). As the tide began to rise (Figure 7d), the $\langle SSC \rangle_x$ and $\langle u \rangle_x$ profiles displayed similar shapes as Low Tide with a smaller range in values. The $\langle SSC \rangle_x$ profile exhibits a more logarithmic shape above the bed and the $\langle u \rangle_x$ profile had a less defined near bed kink when compared to the Low Tide profiles (Figure 7c).

During the Upper Rising tide transects (Figure 7e), $\langle SSC \rangle_x$ and $\langle u \rangle_x$ showed little variation with height above the bed. The value of $\langle u \rangle_x$ was 0.3 m/s at 4 m above the bed and slowly increase linearly to the surface reaching near 0.4 m/s. At 4 m there was a sharp kink in the velocity profile as velocity decreased quickly due to the frictional resistance of the bed. The value of $\langle SSC \rangle_x$ was low and nearly uniform at about 55 mg/L throughout the profile but at 9 m above the bed concentration began decreasing to about 20 mg/L at the surface. Later, during the High Tide transects (Figure 7f), the salt wedge intrusion entered the channel as indicated by the negative $\langle u \rangle_x$ from the bed to about 9 m. Up to 3 m above the bed, $\langle u \rangle_x$ was less negative as friction from the bed forced the saline water to slow. The region of decreased $\langle u \rangle_x$ in the wedge persisted until around the maximum crest height where $\langle u \rangle_x$ remained constant until 5 m above the bed where the velocity slowed again due to the slow moving fresh water above. Values of $\langle WCB_x \rangle$ within the upper fresh water column remained relatively constant but increased towards the bed at the salt wedge due to the salinity gradient. A lack of a mid-profile peak in the $\langle WCB_x \rangle$ profile suggests that flow is heavily mixed as the salt wedge enters the channel preventing a sharp gradient from forming. Mixing between the wedge

and the fresh water is likely heightened by the presence of dunes along the boundary (Kostaschuk et al., 2010).

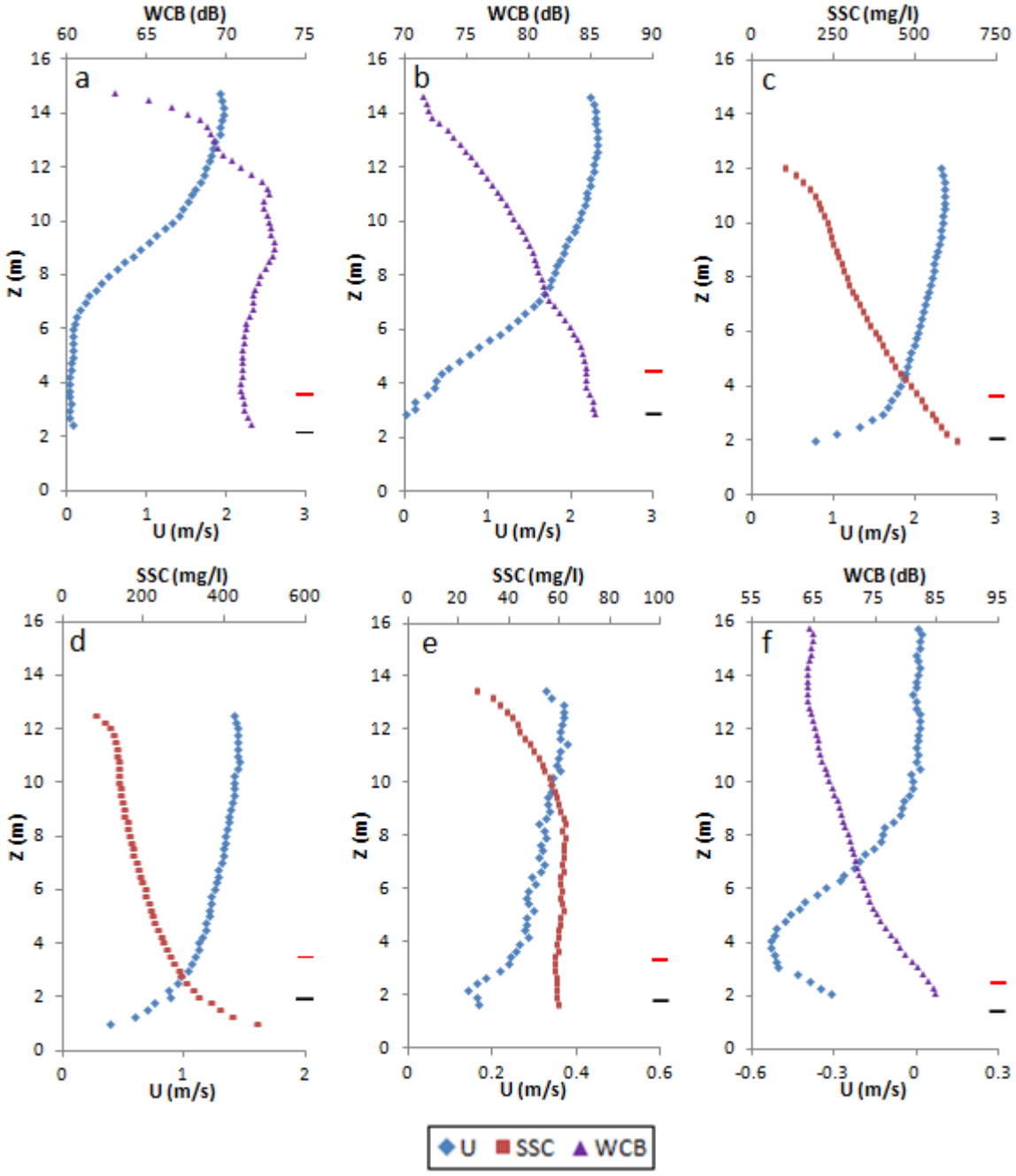

Figure 7. Mean spatially averaged (u), mean suspended sediment concentration (SSC) and/or mean water-corrected backscatter (WCB) above the lowest bed point for select transects within the defined tidal cycle periods: (a) Upper Falling Tide (Transect B); (b) Lower Falling Tide (Transect F); (c) Low Tide (Transect H); (d) Lower Rising Tide (Transect I); (e) Upper Rising Tide (Transect J); and (f) High Tide with Salinity Intrusion (Transect K2). Red ticks indicate the highest bed point along the transect while black ticks show the average bed position.

3.3. Flow structure and sediment concentration over dunes

3.3.1. High Falling Tide

Flow was stratified but the salt wedge was no longer migrating up the channel during the early tidal fall. Values of $\langle WCB'_{xz} \rangle$ ranged from -10 to +12 db (Figure 8a) and revealed a vertical pattern of three distinct layers: a homogeneous fresh water layer in the upper flow, a broad mixing zone around a pycnocline in mid flow and a homogenous saline lower layer. The vertical position of the pycnocline remained relatively constant along the transects, however waveforms that were out of phase with dune wavelengths appeared over larger dunes. Some regions showed evidence of smaller interfacial waves about 10 m in length and 2 m in height that cusped up into the freshwater layer and propagated downstream (Figure 8a, 25-125 m). Tedford et al. (2009) interpreted these wave forms as one-sided Holmboe instabilities. The instabilities appeared over the bedforms suggesting that they may be controlled by the hydraulics of flow over dunes (Tedford et al., 2009; Kostaschuk et al., 2010). However, instabilities did not always form along the interface and the largest and most defined instabilities frequently appeared where the flow converged over the bar.

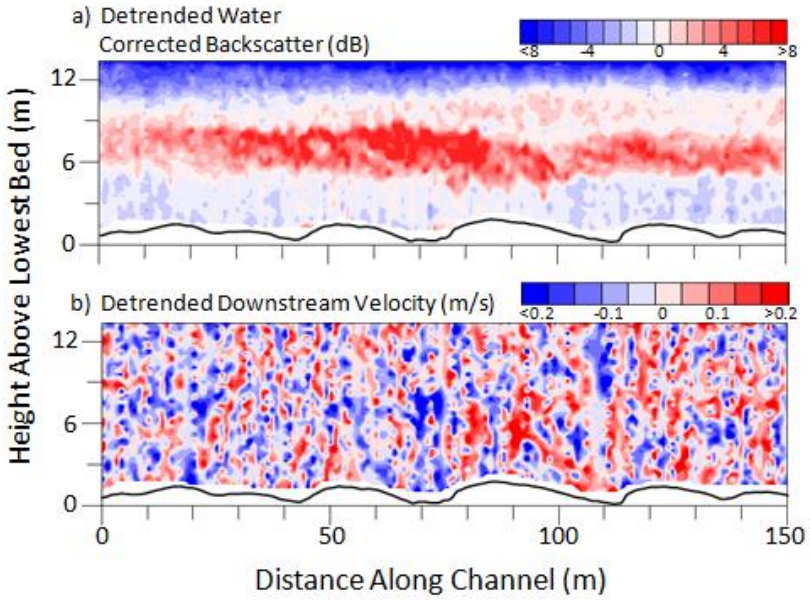

Figure 8. Example from Transect B during the High Falling portion of the tidal cycle: (a) spatially detrended water-corrected backscatter <WCB'$_{xz}$> (dB), (b) vertically-detrended streamwise velocity <u'>$_{xz}$ (m/s). Flow is right to left.

Streamwise velocity deviation from the mean <u'>$_{xz}$ did not show a strong pattern over the dunes (Figure 8b). Regions of highest deviation frequently occurred within the interface layer but these have no clear pattern and were not directly related to instabilities in the <WCB'$_{xz}$>. While the instabilities are revealed in the backscatter, the velocities are not likely resolvable because the aDcp sampling volume at the pycnocline may be too large to capture these events. At ~5 m below the surface, for example, only events with a diameter greater than 4.5 m would be captured in the <u'>$_{xz}$ contour maps.

3.3.2. Low Falling Tide

River flow began to dominate the channel as the tide continued to fall, flushing out the salt wedge and removing the highly stratified flow structure. Deviation in the water-corrected backscatter <WCB'>$_{xz}$ was larger (Figure 9a: -12 to +14 db) than the previous tidal stage and revealed a distinct pattern over the dunes. Figure 9a shows

that positive $\langle WCB' \rangle_{xz}$ dominated the lower half of the water column. The highest deviation in backscatter commonly occurred in the bedform troughs (Figure 9a: 35-50 m), possibly reflecting a combination of saline water (e.g. Geyer and Farmer, 1989) and increased SSC that was trapped in these regions of lower downstream flow velocity. Kostaschuk and Best (2005) suggested that suspended sediment concentrations are high on the falling tide because fine sediment deposited during the low flow velocities at high tide would be readily available for transport. While the increased WCB likely reflects the increased suspended sediment material flux there is no evidence of well-defined individual suspension events in the records which prevented suspended bed material from moving high into the water column.

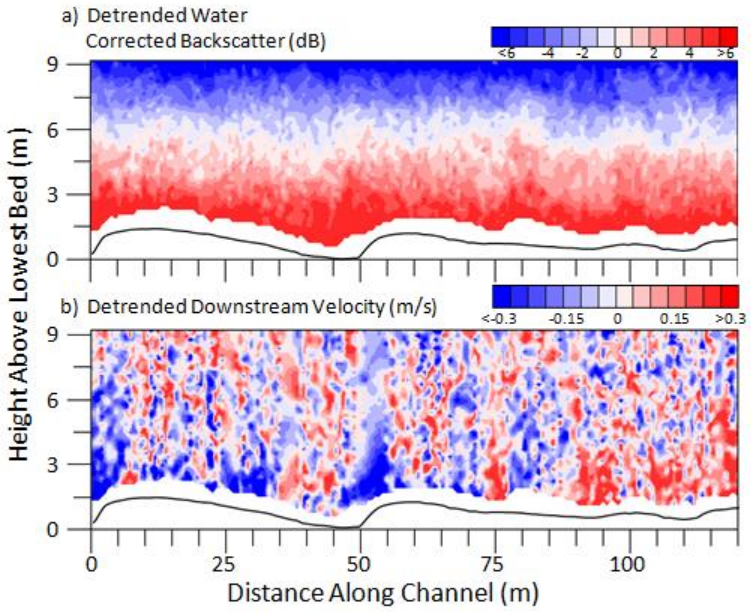

Figure 9. Example from Transect F during the Lower Falling portion of the tidal cycle: (a) spatially detrended water-corrected backscatter $\langle WCB'_{xz} \rangle$ (dB), (b) vertically-detrended streamwise velocity $\langle u' \rangle_{xz}$ (m/s). The difference in the bottom of the aDcp records and the multibeam bed profiles at 75-100 m is due to the difference size of the acoustic footprints at the bed. Flow is right to left.

Values of $\langle u' \rangle_{xz}$ were much larger than previously observed in the tidal cycle (Figure 9b: -0.65 m/s to +0.80 m/s) because the bed began to exert friction on the flow

as it accelerated. Although the contour maps are relatively noisy, flow over larger bedforms (Figure 9b: 50 to 75 m) began to show weak evidence of topographical forcing as the fluid accelerated over the crestal region and decelerated due to expansion in the trough. A larger $\langle u' \rangle_{xz}$ range, especially near the boundary, suggests that the bed began to influence the flow as increased resistance added variability in the velocity that was not observed earlier in the tidal fall.

3.3.3. Low Tide

During Low Tide observations, saline water was completely flushed out of the channel, and downstream velocity and suspended sediment concentrations were the highest observed in the tidal cycle. There were also well-defined suspension events that were spatially variable. Concentrations ranged from 310 mg/l less than the mean to 625 mg/l greater than the mean (Figure 10a). Numerous narrow zones of high $\langle SSC' \rangle_{xz}$ emerged up into the water column from the bed and extended to the surface. These structure were angled into the flow at a mean of 24° with a range from 9° to 42°, but flattened to lower angles in the upper flow where downstream velocity is greater. Values of $\langle SSC' \rangle_{xz}$ within individual events were highly variable with some of the better defined events (Figure 10a: 40 & 60 m) deviating up to 600 mg/l from the mean. Numerous suspension events formed over individual dunes making it difficult to distinguish between events and to determine their origins in relation to the dunes, although they tend to emerge at the lower to mid-stoss region and over the lee of the bedforms. Suspension events over the lower stoss appeared low in the water column but increased in height over the stoss until reaching near the surface downstream of the crest (Figure 10a: 75-100 m). Other large events, such as those at 60 m and 20 m in Figure 10a, emerged over the lower lee and trough.

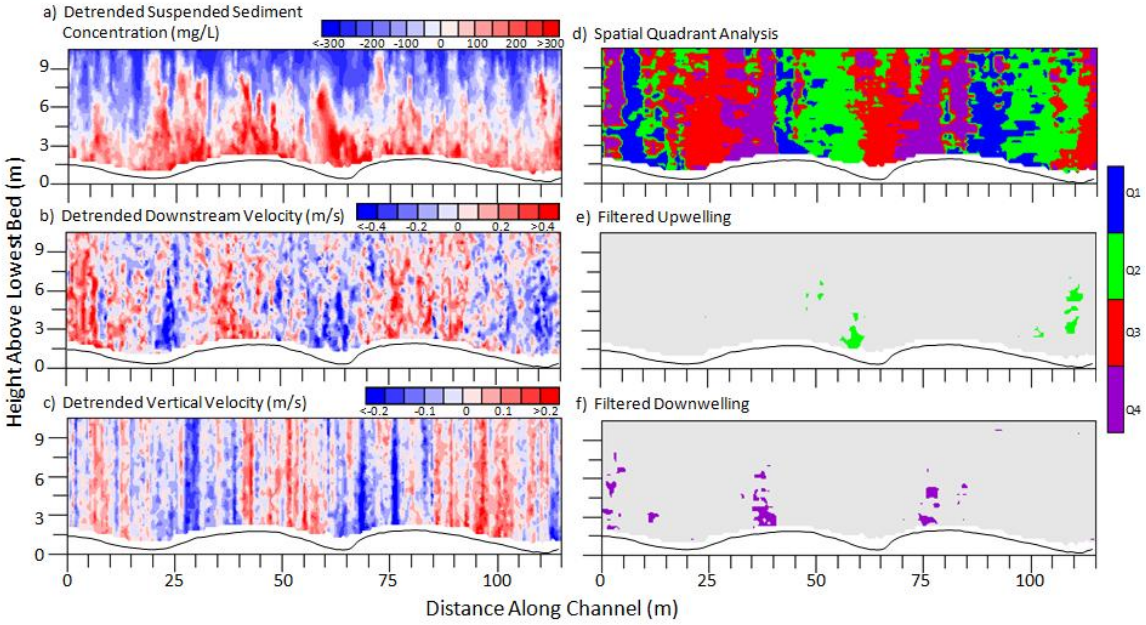

Figure 10. Example from Transect H during the Low Tide portion of the tidal cycle: (a) spatially detrended suspended sediment concentration $\langle SSC' \rangle_{xz}$ (mg/L), (b) vertically-detrended streamwise velocity $\langle u' \rangle_{xz}$ (m/s), (c) vertically-detrended vertical velocity $\langle w' \rangle_{xz}$ (m/s), (d) spatial quadrant analysis (dB), (e) intensity filtered upwelling regions, (f) intensity filtered downwelling regions. Flow is right to left.

Flow characteristics of the suspension events were not well captured in the velocity records. Spatially detrended streamwise velocity $\langle u' \rangle_{xz}$ ranges from -0.80 to 0.80 m/s (Figure 10b) and generally displayed patterns consistent with topographical forcing. Well-defined spatial regions of slow downstream flow occurred in dune troughs, extending from the lower lee to the lower stoss where flow accelerated up the stoss (Figure 10b: 50-70 m). The largest positive $\langle u' \rangle_{xz}$ frequently occurred along the stoss and at the crest where flow converges (Figure 10b: 70-95 m). The largest range in $\langle u' \rangle_{xz}$ frequently occurred lower in the flow revealing a strong influence of the bed. Spatially detrended vertical velocity $\langle w' \rangle_{xz}$ was positive as fluid was forced over the stoss and negative as it moved down the lee. While individual events in the $\langle SSC' \rangle_{xz}$ records are not reflected in the velocity records, larger positive deviations in $\langle SSC' \rangle_{xz}$ frequently coincided with zones of larger negative $\langle u' \rangle_{xz}$ (Figure 10b: 60 m).

Spatial quadrant analysis (Figure 10d) showed a consistent pattern of upwelling (Q2) and downwelling (Q4) with little variability between individual dunes. Upwelling regions began at the lower stoss and ended at the crestal region. Downwelling occurred over the crest and extended down into the mid-lee region. Higher intensity upwelling (Figure 10e) and downwelling (Figure 10f) are limited to much smaller spatial areas and are commonly found near the bed rather than high in the flow. Intense upwelling regions appeared on the lower stoss where the fluid converged and were forced up over the bedforms. High intensity downwelling zones appeared at the crest or over the upper lee where flow expanded and moved toward the bed.

3.3.4. Low Rising Tide

Downstream velocity steadily decreased as the tide rose. While the $\langle SSC' \rangle_{xz}$ was lower than the previous stage (Figure 11a: -145 to +190 mg/l), easily identifiable large-scale suspension events were apparent near the bed and maintained their shape towards the surface (Figure 11a). The structures appeared less frequently than events observed during Low Tide but are similarly angled into the flow at a mean of 25° and a range from 14° to 42°. Strong positive $\langle SSC' \rangle_{xz}$ occurred at the lower stoss where structures grew above the bed until reaching the flow surface over the bedform upper stoss or crest (Figure 11a: 60 m to 70 m). Some events emerged at the crest and lower lee, although they were less frequent than those observed at low tide. Bedform troughs and lee sides often displayed large concentrations of suspended sediment near bed (Figure 11a: 25 to 45 m). Kostaschuk and Villard (1996) suggested that high concentrations of sand in suspension leads to increased deposition in dune troughs and Kostaschuk and Best (2005) showed increased sand falling out of suspension as tides started to rise. It is likely that these zones of high $\langle SSC' \rangle_{xz}$ are related to sediment

falling out of suspension from events that extended over the bedform immediately upstream.

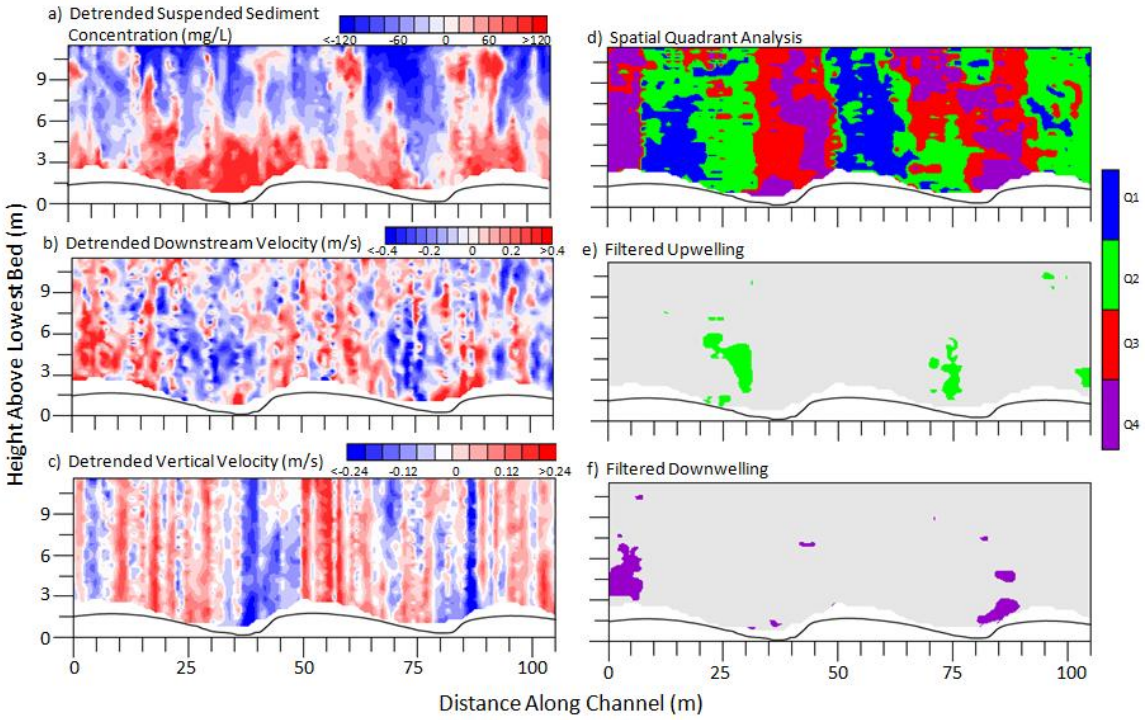

Figure 11. Example from Transect I during Lower Rising portion of the tidal cycle: (a) spatially detrended suspended sediment concentration $\langle SSC' \rangle_{xz}$, (b) vertically-detrended streamwise velocity $\langle u' \rangle_{xz}$ (m/s), (c) vertically-detrended vertical velocity $\langle w' \rangle_{xz}$ (m/s), (d) spatial quadrant analysis, (e) intensity filtered upwelling regions, (f) intensity filtered downwelling regions. Flow is right to left.

The spatial pattern in $\langle u' \rangle_{xz}$ was consistent with the topographical forcing observed during the Low Tide transects, although the range in $\langle u' \rangle_{xz}$ was smaller (Figure 11b: -0.60 to +0.60 m/s). Regions of downstream-titled decelerated flow emerge out of the troughs and over stoss dunes (Figure 11b, 15-40 m) providing evidence of larger scale flow structures in the $\langle u \rangle_{xz}$ measurements. As the decelerated downstream fluid moved over the dunes, it was angled up into the flow as it entered the zone of positive vertical velocity. Large well-defined suspension events appear to be strongly related to the upwelling regions.

Spatial quadrant patterns were similar to those during Low Tide, although upwelling and downwelling regions were more clearly tilted into the flow and occupied more coherent spatial zones over the bedforms (Figure 11d). Upwelling regions frequently appeared over the lower stoss and were titled up into the flow while downwelling occurred downstream of the crest and over the lee. Application of the intensity filter to upwelling (Figure 11e) and downwelling (Figure 11f) regions revealed that these zones occupied a relatively large spatial area, suggesting greater coherency than at Low Tide. The upwelling zones emerged from the trough, were titled up into the water column and extended higher up towards the surface. These higher intensity upwelling regions were also frequently detached from the bed, providing evidence that these may be signatures of large coherent structures that evolve from the boundary up into the flow, similar to the events observed by Shugar et el. (2010). Downwelling regions were observed higher up in the flow were also titled in the downstream direction.

3.3.5. High Rising Tide

As downstream velocity in the channel decelerated approaching high tide, patterns in the velocity and suspended sediment records were less apparent. Values of $\langle SSC' \rangle_{xz}$ ranged from -33 to +49 mg/l (Figure 12a) with weak evidence of the suspension patterns events that dominated the previous two tidal stages. Regions of higher $\langle SSC' \rangle_{xz}$ occurred over the crests. Decreased flow velocity suggests that bed material entrainment had likely stopped and the SSC consisted of fine material remaining in suspension from the previous tidal stage. Streamwise velocity deviations from the mean $\langle u' \rangle_{xz}$ (Figure 12b) were low at -0.5 to +0.5 m/s and were highly variable. Higher $\langle u' \rangle_{xz}$ occurred over the crests and slower flow velocity was evident in the trough, although this pattern is much less defined compared to the previous two tidal stages.

There was a weak pattern of positive $\langle w' \rangle_{xz}$ over the stoss of the dunes and negative $\langle w' \rangle_{xz}$ over the lee but the range of $\langle w' \rangle_{xz}$ was low (Figure 12c: -0.12 to 0.12 m/s). The spatial quadrant analysis (Figure 12d) showed a weak pattern similar to those observed in the previous tidal stages although the low $\langle w' \rangle_{xz}$ values resulted in some contamination from vertical motion of the boat. Application of the intensity filter to regions of upwelling (Figure 12e) and downwelling (Figure 12f) confirmed that the patterns in the flow were weak as intense regions were scattered above the bed and did not reveal any coherency.

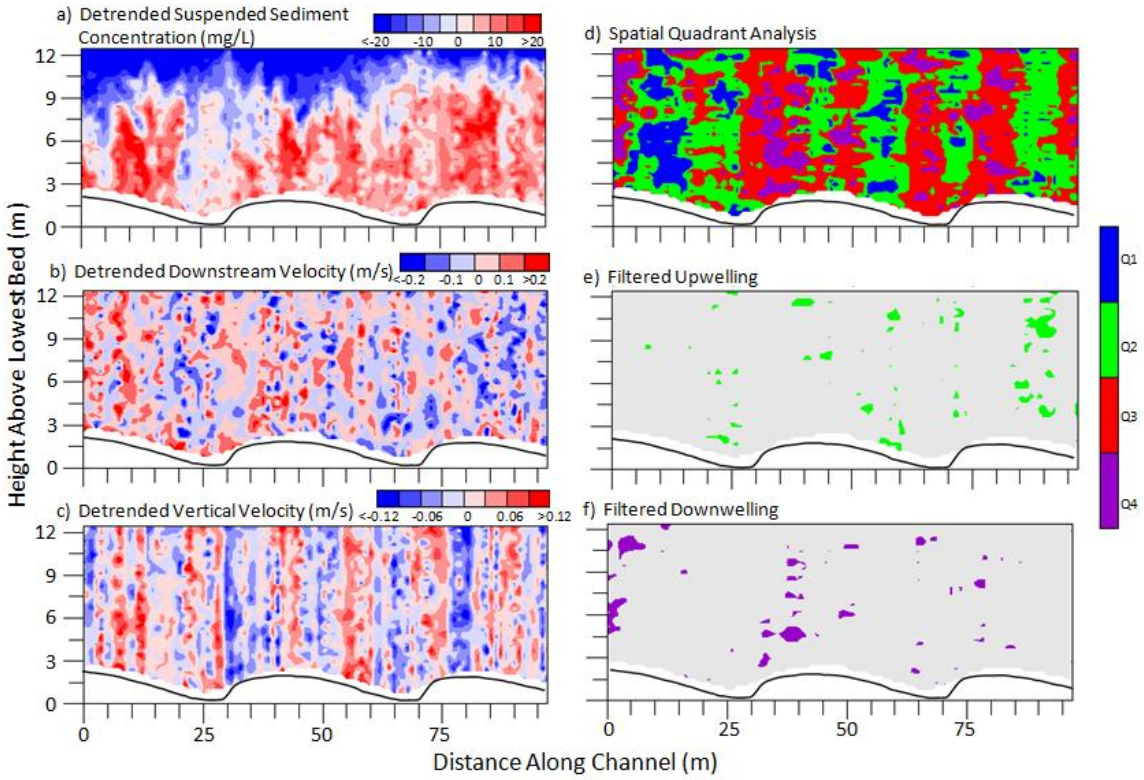

Figure 12. Example from Transect J during High Rising portion of the tidal cycle: (a) spatially detrended suspended sediment concentration $\langle SSC' \rangle_{xz}$, (b) vertically- detrended streamwise velocity $\langle u' \rangle_{xz}$ (m/s), (c) vertically-detrended vertical velocity $\langle w' \rangle_{xz}$ (m/s), (d) spatial quadrant analysis, (e) intensity filtered upwelling regions, (f) intensity filtered downwelling regions. Flow is right to left.

3.3.6. High Tide

The upstream migration of the salt wedge was clearly apparent in the $\langle WCB' \rangle_{xz}$ record at High Tide (Figure 13a). The front of the wedge (Figure 13a: 690 m) appeared as a distinct plume clearly defined by the sharp peak in $\langle WCB' \rangle_{xz}$ due to the strong density gradient between the fresh and salt water. From the front of the wedge until about 140 m (Figure 13a) the interface of the wedge sloped upward until it reached near the surface at about 13 m above the bed where it remained at a constant height. The $\langle WCB' \rangle_{xz}$ record (Figure 13a) shows plumes of increased backscatter that extended up into the water column as saline water was topographically lifted towards the surface over the

dunes, as described by Kostaschuk et al. (2010). Higher up in the water column, these plumes were titled in the downstream direction as they mixed with the slowly moving, downstream-directed fresh water above. Further downstream, $\langle WCB' \rangle_{xz}$ decreased but remained positive suggesting that more mixing was occurring between the fresh and saline water that prevented a sharp density gradient from forming.

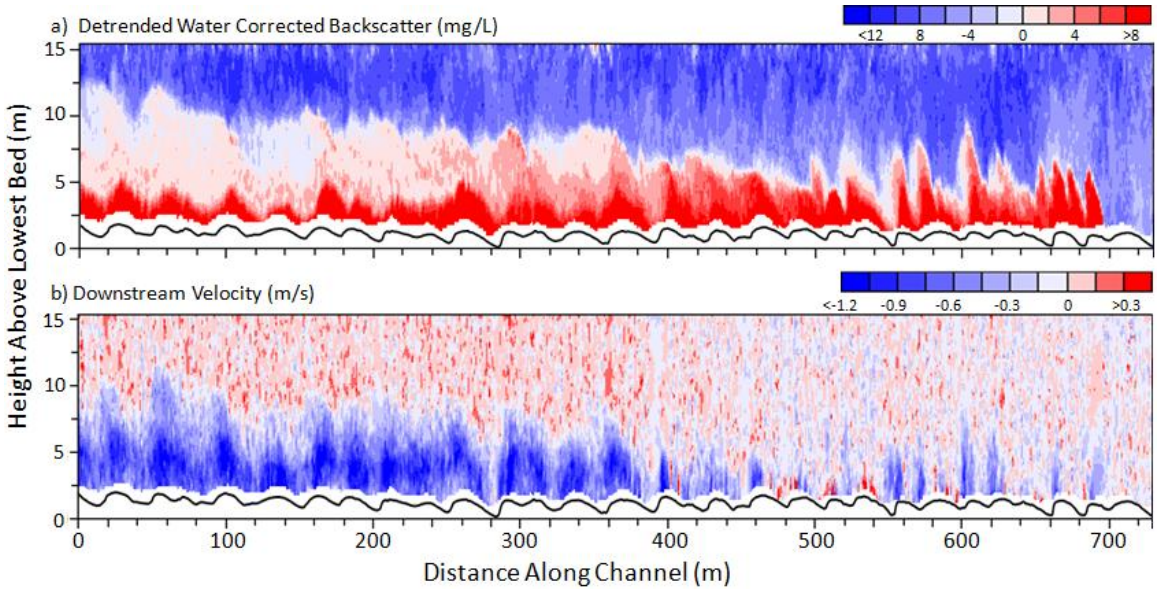

Figure 13. Example from Transect K2 during the High Tide portion of the tidal cycle: (a) total suspended sediment concentration $\langle WCB'_{xz} \rangle$ (mg/L), (b) Downstream Velocity u_{xz} (m/s). River flow is right to left.

Figure 13b shows the downstream velocity as recorded by the aDcp. I display the downstream velocity rather than the detrended downstream velocity because there is a strong streamwise gradient in velocity, making detrended data difficult to interpret. Negative velocities in the flow field reveal that the salt wedge is moving upstream, opposing the downstream moving fresh water above. Flow within the salt wedge displayed a distinct pattern while the relatively slower moving fresh water above showed little pattern. At the head of the salt wedge, velocity ranges from about -0.3 to -0.6 m/s (upstream flow) but further downstream within the salt wedge velocity approaches -1.5

m/s. The decreased upstream velocity at the head of the wedge was likely due to the resistance from the downstream flowing fresh water. Velocity within the wedge over bedforms is more negative than over the troughs because topographic forcing caused the saline water to accelerate over dune crests and decelerate in the troughs. Topographic forcing shows a reverse pattern to that observed at low tide as acceleration and uplift occurred over the stoss and deceleration occurred over the lee.

4. Discussion

4.1. How does the mean flow structure change over low-angle dunes with unsteady flow?

The mean flow structure over low-angle dunes underwent significant change through the tidal cycles. During the upper rising to high tide, flow in the channel decelerated and nearly stopped with no clear patterns in the mean flow structure until the salt wedge rapidly entered the channel. Accelerated and upward directed fluid motion over dune lee slopes and decelerated downward motion over stoss slopes reveal the influence of dune topography on the salt-wedge intrusion as in Kostaschuk et al. (2010). Saline fluid forced upwards over dunes was tilted downstream in the fresh water flow causing plumes in the $\langle WCB' \rangle_{xz}$ that were more pronounced at the wedge front (Figure 13a: 690 m). Enhanced mixing downstream of the wedge front produced larger, less well-defined plumes. Interfacial waves along the saline-fresh water interface were in-phase with the bedform crests.

Early in the falling tide flow was stratified with an upper fresh water layer and a lower saline layer, separated by a mixing layer. Flow within the saline layer was positive in the downstream direction suggesting that the salt wedge was beginning to exit the channel due to a downstream longitudinal pressure gradient. Tedford et al. (2009) showed that these asymmetric instabilities were dominantly one-sided Holmboe modes formed along the saline-fresh water interface due to unstable interaction of density and velocity gradients. MacDonald and Horner-Devine (2008) and Tedford et al. (2009) both

argued that bottom friction retards the out flowing salt wedge, which promotes increased shear along the saline-fresh water interface causing instabilities and increased mixing.

A well-defined region of instabilities appeared on the falling tide as flow moved over the bar while instabilities were mostly absent outside of this region. Geyer and Farmer, (1989) showed that mixing is enhanced where flow accelerated in the channel so it is possible that the acceleration of the flow over the bar promoted the observed instabilities observed instabilities. Tedford et al. (2009) suggested that instabilities may not appear in measurements if vessel velocity is not appropriate relative to the speed of the instabilities. This may explain the absence of well-defined instabilities outside of the flow converging over the bar.

During lower falling tide, river flow began to flush out the saline water and eliminated stratified flow. Higher $\langle WCB' \rangle_{xz}$ in the bedforms troughs may be related to pockets of saltwater previously observed by Geyer and Farmer (1989) on falling tides. However, $\langle WCB' \rangle_{xz}$ in the dune troughs was higher than previously observed at the pycnocline, suggesting that suspended sediment $\langle SSC \rangle_{xz}$ also contributed to the $\langle WCB' \rangle_{xz}$. Kostaschuk (2002) also noted an increase in near bed suspended sediment concentration as the salinity intrusion was pushed out of the channel. Fine sediment deposited during the near slack water at high tide would be readily available for transport as flow in the river begins to accelerate. Higher $\langle WCB' \rangle_{xz}$ may also occur in dune troughs due to increased scour during the falling tide (c.f. Kostaschuk and Best, 2005).

River flow dominated the channel at low tide. Flow over the low-angle dunes was topographically influenced as flow acceleration occurred over the stoss and deceleration occurred in the lee side. Fluid was forced upwards from the lower stoss to the crestal

region and moved towards the bed in the lee and the trough regions. These topographical induced patterns were consistent throughout the Low Tide transects and agree well with the mean velocity characteristics over low angle dunes observed by Kostaschuk and Villard (1996; 1999) and Best and Kostaschuk (2002). The measurements showed no evidence of flow separation past the crest in agreement with previous observations that the low-angle lee slopes do not produce permanent flow separation (e.g. Kostaschuk and Villard, 1996; Best and Kostaschuk, 2002), although aDcp beam geometry may result in spatial averaging volumes too large to capture the separated flow (Kostaschuk et al. 2004, Parsons et al. 2005).

The spatial quadrant analysis showed upwelling (Q2) over the lower stoss and downwelling (Q4) at the crest or down the lee during the low and low rising tide observations. Zones of intense upwelling at the lower stoss and downwelling at the crest consistently appeared close to the bed. The location of these zones over dunes agree well with the model described by Kostaschuk and Villard (1999). They suggested that 'sweep-like' structures are followed be 'ejection-like' structures at the crest and at the point of separation. While the persistent downwelling is not followed by upwelling at the crest and upwelling is not preceded by downwelling at the stoss, the intense regions occur over the dunes in nearly identical locations to those proposed by Kostaschuk and Villard (1999).

The mean flow field on the rising tide was influenced by dunes in a fashion similar to low tide. However, one notable difference was that the decelerated zone of flow in the troughs extended up into the flow and was tilted downstream over the stoss of the next downstream bedform. Regions of intense upwelling were also more coherent and occupied a larger area compared to low tide. These observations may reflect the

enhanced turbulence that occurs in estuaries during rising tides (Gordon, 1975; Kostaschuk et al. 1989; Best and Kostaschuk, 2005) due to variation in longitudinal pressure gradients caused by tidal flow (Davies, 1977). Thus, even though flow velocities were higher during low tide, there was less evidence of macroturbulence in the measurements because turbulence intensity may have been suppressed. Strong mixing in the low tide flow fields may also have prevented large-scale turbulence production and promoted smaller scale events that were occurring too frequently to be captured by the aDcp sampling frequency or were much smaller than the sampling volumes of the instrument.

Most observations of flow over dunes have been in flumes with unidirectional flow and asymmetric high-angle dunes with lee angles around 30° (eg. Bennett and Best, 1995; McLean et al., 1994; Best, 2005b). Comparison between high-angle and low-angle dunes from this study are limited to Low Tide and Upper Rising tide transects as flow is more intimately coupled to the bed during these stages. Mean flow patterns over high-angle dunes are typically topographically influenced with permanent flow reversal and strong flow recirculation (e.g. Venditti and Bennett, 2000). While flow over the low-angle dunes in this study was strongly influenced by bed topography, the most significant difference from high-angle dunes is the apparent absence of flow separation in the lee and trough. This region experienced flow deceleration but no upstream velocities were measured. This observation agrees with Best and Kostaschuk (2002) who showed the absence of permanent flow separation over a dune with a lee-side of 14° in their flume study using a laser Doppler anemometer. They did, however, observe highly-intermittent near bed flow reversal in time series that was not captured in my measurements.

4.2. What are the characteristics of suspension events and how do they evolve over low-angle dunes?

The $\langle SSC' \rangle_{xz}$ contour maps during Low and Lower Rising tide show that flow was dominated by large-scale suspension events that carried much higher sediment concentrations than the ambient flow around them. These events formed near the bed and grew up into the flow as relatively narrow structures, tilted downstream at a mean angle of about 25°. During low tide, suspension events appeared more numerous over the dunes than any other period in the tidal cycle, appearing over nearly all dunes regardless of individual morphological characteristics. Kostaschuk and Best (2005) argued that enhanced turbulence on the rising tide may result in increased sediment suspension. These results show that as the tides begin to rise, suspension events emerged as larger structures in the flow suggesting that turbulence was enhanced however, suspended sediment concentrations were smaller than at low tide.

Through the semi-Eulerian framework adopted for these measurements, I can infer where the suspended sediment events occurred over the dunes and how they evolved in the water column by examining individual suspension events that occur in a sequence in the $\langle SSC' \rangle_{xz}$ flow field maps. The observations show that events originated in two main regions over the dunes: immediately downstream of the crest over the upper lee and more frequently at the lower stoss. Suspension events consistently appeared low in the water column at the lower stoss. Further up over the stoss and past the crest, events appeared to grow higher up in the water column suggesting that they were anchored to the bed morphology and that their generation was not a random process. This observation suggests that the sediment suspension events begin at the lower stoss at the region of intense upwelling and grow in size up over the bedform towards the

surface where they break down in the decelerate flow region over the trough. High $\langle SSC' \rangle_{xz}$ over dune lees and troughs, particularly on the rising tide, did not appear as narrow structures up into the flow but rather as longer regions confined to the trough in the lower water column. Kostaschuk and Villard (1996; 1999) suggest that this may be due to the sediment falling out of suspension as velocity decelerated and ejection events dissipated. My observations are consistent with this interpretation. In addition to events that emerge at the lower stoss, I also observed distinct suspension events that occurred immediately after dune crests. These had similar structures to the events that over the stoss but appeared as individual events rather than in a sequence and were not as commonly found over the dunes. Suspension events over the upper lee may occur intermittently because they were not persistently found over all the dunes.

A direct linkage between the suspension events and a specific fluid structure cannot be made with my data because the sampling volume of the aDcp is too large relative to the structures in order to resolve internal velocities. However, Kostaschuk and Church (1993) observed similar features in the flow using acoustic profilers which they interpreted as macroturbulent kolks that entrained and transported large volumes of bed-material. Using a current meter, they showed that kolks had signatures of ejections with negative fluctuation from a time-averaged downstream mean velocity and positive fluctuation from the mean vertical velocity. They attributed this signature to the upwelling of slower near-bed fluid that was observed to emerge on the lower stoss and grow up over dunes. My observations of flow and suspended sediment events are consistent with those Kostaschuk and Church (1993). Events with the highest positive $\langle SSC' \rangle_{xz}$ frequently coincided with zones of larger negative $\langle u' \rangle_{xz}$ (Figure 10b: 60 m) suggesting that the instrument was capturing ejection-like fluid signatures. This signal was more

pronounced on the lower rising tide as turbulence appeared enhanced in the water column. Large well-defined suspension events observed in the $\langle SSC' \rangle_{xz}$ appear to be related to the upwelling regions and even more strongly related to negative $\langle u' \rangle_{xz}$ regions in the flow (Figure 11b, 15-40 m).

If these suspension events observed in the $\langle SSC' \rangle_{xz}$ are large-scale macroturbulent-kolk structures, the spatial characteristics of the events reveal something about the dynamics of kolks. Sediment suspension events that appeared low in the flow at the lower stoss but grew in height over the dunes and dissipated beyond dune crests are consistent with Best and Kostaschuk's (2002) explanation of low-angle dune kolk generation. They suggest that instabilities may form along a weak shear layer between the main flow and decelerated flow in the trough. When these instabilities reach the point of reattachment, they could coalesce into the region of intense upwelling at the lower stoss and grow up into flow as macroturbulence. The suggestion by Best and Kostaschuk (2002) that intermittent flow separation may develop K-H instabilities that produce low magnitude and intermittent eddy generation may also provide a mechanism for suspension events observed after the crest. However, the hypothesis that 'burst' events within the turbulent boundary layer (Jackson, 1976) grow through the autogeneration of hairpins vortices (Adrian, 2007) is also a reasonable explanation for the suspension events observed here, especially for the events that grow up over the stoss of dunes. It is clear that additional research is required to resolve the origin of coherent structures that emerge over low-angle dunes and flat beds. Controlled flume experiments that provide time-resolved, spatially explicit observations of the flow and observations of the water surface deformation, may provide useful insights into the origin of macroturbulence that influence sediment suspension events.

4.3. What is the linkage between sediment suspension and flow over low-angle dunes?

Intense persistent regions of downwelling and upwelling in the flow may be responsible for the sediment suspension events observed over these low-angle dunes. Kostaschuk and Villard (1999) suggested that turbulent 'sweep-like' structures that impinge the bed at the dune crest and at the point of reattachment erode bed sediment which is then suspended by 'ejection-like' structures, or kolks. When suspension events appeared in the suspended sediment records, the spatial quadrant analysis showed patterns of persistent downwelling at the crest and upwelling at the lower stoss in similar locations to those proposed by Kostaschuk and Villard (1999). The downwelling zones at the crest observed in my data are likely associated with sweep-like motions that erode bed material which is then transported downstream close to the bed by the mean flow. Zones of upwelling, where ejection-like motions are commonly observed, are associated with periodic suspension of sediment (Figure 10a: 30 m). Since permanent flow separation does not occur on the lee side, these observations suggest that bed material mobilized by the sweeps, but is not suspended into the flow at the brinkpoint, will continue to move downstream close to the bed in the deceleration zone (Figure 11a: 25-40m). The bed slope in this region assists in maintaining sediment transport. This material could then be available for suspension by periodic ejections that are generated in the zone of upwelling at the reattachment of the deceleration zone on the lower stoss side of the downstream dune (Figure 11a: 20 m).

Previous work has qualitatively assessed how large-scale suspension events contribute to sediment flux in rivers and it is it is widely accepted that macroturbulent events such as kolks are capable of transporting large volumes of suspended sediment

(c.f. Rood and Hickin, 1989; Kostaschuk and Church, 1993; Kostaschuk and Villard, 1999; Venditti and Bennett, 2000; Best, 2005a; Shugar et al., 2010). However, a quantitative understanding of how much large-scale suspension events contribute to sediment flux is absent in the literature. Observations at low and low rising tide support the notion that large suspension events are major agents of suspended sediment transport. Figure 14 shows the distribution of suspended sediment concentration deviation from the mean and median at low tide (Transect M) and high tide (Transect K). Using the mean or the median provides a useful method to delineate sediment suspension events from the rest of the flow and selecting the median rather than the mean has no significant effect on the patterns in Figure 10a, 11a, 12a. Figure 14a shows that when suspension events are present over the dunes at low tide, the distribution in the flow field is skewed towards higher concentrations with a pronounced high concentration tail. When the well-defined events are absent at high tide (Figure 14b), the observations are normally distributed. The skewness towards higher concentrations and the high concentration tail in Figure 14a suggest that higher concentrations are carried in a smaller total volume over the dunes at low tide.

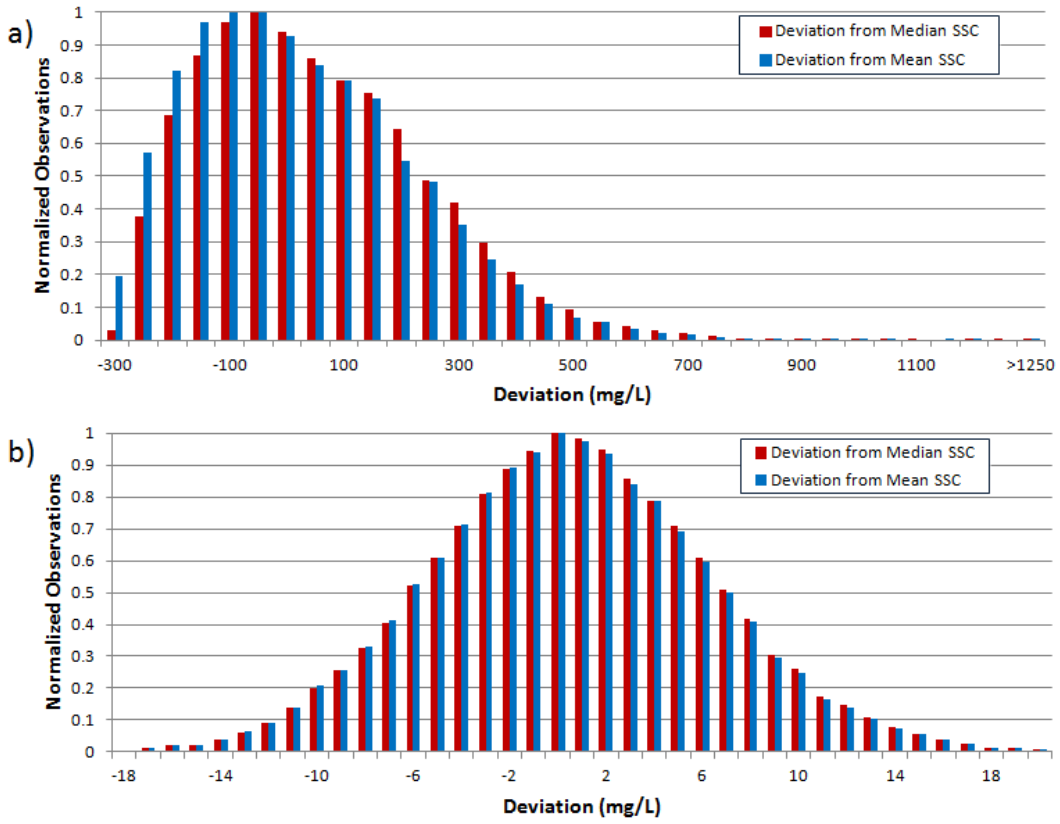

Figure 14. Distribution of the deviation from median suspended sediment concentration SSC (red) and deviation from mean suspended sediment concentration SSC (blue) observations. (a) is Transect M at low tide where the flow is dominated by suspension events and (b) is Transect K at high tide when suspended sediment concentrations are low and no events are present in the flow fields.

The suspended sediment concentration fields (e.g. Figure 10a, 11a, 12a) allow me to further quantify how suspension events affect the suspended sediment concentrations. For each transect, I calculated the total sediment in suspension over the dunes V_T by summing the volume of sediment carried in each h_i-by-l_i cell (where h_i = 0.25 m and l_i = average distance between ensembles for the transect):

$$V_T = \sum C_i A_i w_i \qquad (18)$$

where C_i is the suspended sediment concentration in each cell (in mg/m^3), A_i is the area (m^2) of each cell and w_i is the width of each cell (assumed to be 1 m, a unit width). I first

used equation 18 to calculate the total sediment volume in suspension V_T. Then I calculated the volume in cells that had concentrations greater than the mean $V{>}\mu$ and less than the mean $V{<}\mu$. As such, changes in the ratio of $V{>}\mu$ / V_T highlights the way that suspension events affect sediment concentrations in the channel. Care needs to be taken when interpreting this calculation. Suspension events will tend to increase the bed material concentration in the flow, so without separating bed material from wash material, I cannot calculate the amount of sediment suspended in an individual event from the bed without making some assumptions about the cell specific wash material load. I also need to be careful near the bed, because some cells may have bed material in suspension that is not associated with these events. Nevertheless, examination of $V{>}\mu/V_T$ reveals the effect of having large suspension events in the flow relative to when they are absent.

Figure 15a shows the ratio $V{>}\mu/V_T$ for each transect as well as the ratio of the area of the flow with concentrations greater than the mean relative to the total area of the flow transect ($A{>}\mu/A_T$). That ratio of $V{>}\mu/V_T$ is always greater than 50%, which indicates that the distribution of concentrations in the flow field is always skewed towards higher concentrations, whether the suspension events are present or absent. However, more sediment is transported by a smaller volume of the fluid compared to High Rising and High Tide when suspension events are absent (Figure 15a). This pattern is more obvious when the threshold used to define suspension events in the flow is selected as the median rather than the mean because $A{>}\mu/A_T$ varies depending on the mean concentration. Figure 15b shows the ratio of the volume of sediment carried in cells with concentrations greater than the median V/M relative to V_T. At Low Tide, when the flow is dominated by suspension events, ~69% of the total sediment is carried in 50% of the

flow. As tides begin to rise and suspension events become less frequent but are more coherent, $V_{>M/V_T}$ decreased to 67%. When clearly defined events stop emerging over the dunes at High Rising Tide, but finer sediment is likely still in suspension, 59% of the total sediment is carried in 50% of the flow. This decreased to 58% at High Tide when sediment is depositing out of the water column. While the amount carried in the flow is positively skewed for each of the transects (e.g. Figure 15), these results suggest that more sediment is carried in a smaller volume of water at low tides than at higher tides, quantitatively indicating that these suspension events are indeed responsible for a large portion of the sediment in suspension.

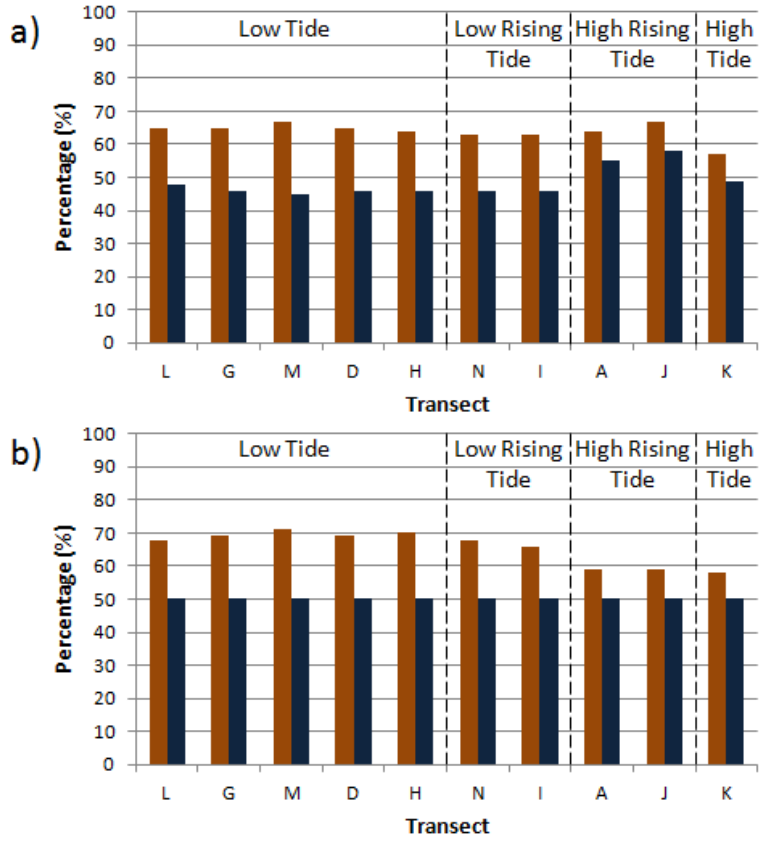

Figure 15. a) The percent of sediment volume carried in cells with concentrations greater than the mean (V>μ) relative to the sum of the total sediment volume (V_T) and the percent area of the transect with concentrations greater than the mean (A>μ) relative to the total transect area A_T. b) The same as panel a, but using the percent of sediment volume carried in cells with concentrations greater than the median (V>M) rather than the mean and the percent area of the transect with concentrations greater than the median (A>M) relative to A_T. By definition A>M/ A_T = 0. Brown bars represent V>μ/ V_T and V>M/V_T. Blue represents A>μ/A_T and A>M/A_T.

While Figure 15 provides a quantitative measure of how sediment suspension events affect the volume of sediment transported in the channel, further work needs to focus on grain-size separation of bed-material (sand) and wash-load (silt-clay) within the water column to determine how much sediment flux can be attributed to individual suspension events. Observations of in-situ, suspended, grain-size dependent flux and aDcp backscatter as suspension events pass should provide a method to accomplish this goal. However, better event detection and identification methods are needed as well, which will require new instrumentation with smaller sampling volumes than the

aDcp to properly resolve the fluid signatures of individual suspension events. Nevertheless, the difference observed in the volume of sediment in the water column with suspension events and without events present provides some quantitative evidence of their effect on sediment concentrations over low-angle dunes.

5. Conclusions

Mean flow and suspension events in unsteady flow were examined in a tidally-influenced reach of the Fraser River, British Columbia, Canada. Dunes displayed low-angle (<30°) lee sides typical of dunes in large sand-bedded rivers, rather than the angle-of-repose asymmetric geometry typical of small channels and flumes. Flow and suspended sediment transport patterns were variable through tidal cycles but reoccurring patterns showed the following:

(1) At high tide, a salinity intrusion entered the channel and plumes of saline water were forced up over the dunes into the downstream moving freshwater due to topographic forcing. The salt wedge persisted in the channel promoting stratified flow with one-sided instabilities forming along the saline-fresh water interface.

(2) River processes dominated over the salt wedge and forced the saline water out of the channel as tides approached the minimum stage. Velocity and suspended sediment concentrations peaked at low tide but decreased as the tides rose.

(3) Flow observations over the low-angle dunes agreed well with previous studies and displayed similar patterns of topographic forcing to those observed over high-angle dunes. However, unlike flow over high-angle dunes, I found no evidence of strong separated flow or flow reversal.

(4) Velocity records showed limited evidence of large coherent flow structures in the flow but large-scale suspension events were captured well in the suspended sediment records during low tide and lower rising. Suspension events dominated the suspended sediment fields at low tide and became less frequent but more coherent as the tide began to rise

(5) Suspension events emerged on the lower stoss side of dunes and grew up over the bedforms and also formed downstream of the crest, although less commonly.

(6) The suspension events carry more sediment than the ambient fluid over dunes. I estimate that 69% of the total sediment is carried by 50% of the flow during low tide when suspension events dominate the flow field.

This study illustrates how the mean flow field changes over low-angle dunes under unsteady flow associated with tidal cycles, reveals patterns of suspension events over low-angle dunes and shows that the events are important in sediment transport. This study, as with many field studies, is limited by a lack of detailed measurements, particularly in the near bed region. Studies such as this need to be coupled with controlled flume experiments and numerical simulations in order to resolve the origin of coherent structures at finer scales and determine how these structures interact with the bed to suspend bed material.

References

Adrian, R. J. (2007), Hairpin vortex organization in wall turbulence. *Phys. of Fluids, 19,* 041301, doi: 10.1063/1.2717527.

Babakaiff, C. S., and E. J. Hickin (1996), Coherent flow structures in Squamish River Estuary, British Columbia, Canada, in Coherent Flow Structures in Open Channels, edited by P. J. Ashworth et al., pp. 321– 342, John Wiley, Hoboken, N. J.

Best, J.L. (2005a), The fluid dynamics of river dunes: a review and some future research directions. *J. Geophys. Res., 110*, F04S02, doi:10.1029/ 2004JF000218.

Best, J.L. (2005b), The kinematics, topology and significance of dune related macroturbulence: some observations from the laboratory and field, in *Fluvial Sedimentology VII. Special Publication*, edited by M.D. Blum, S.B., Marriott, S. Leclair, *Spec. Publ. Int. Assoc. Sedimentol., 35*, 41–60.

Best, J. L., and R. A. Kostaschuk (2002), An experimental study of turbulent flow over a low-angle dune. *J. Geophys. Res., 107 (C9)*, 3135. doi:10.1029/ 2000JC000294.

Best, J., Simmons, S., Parsons, D., Oberg, K., Czuba, J., and C. Malzone (2010), A new methodology for the quantitative visualization of coherent flow structures in alluvial channels using multibeam echo-sounding (MBES), *Geophys. Res. Lett., 37*, L06405,doi:10.1029/2009GL041852

Bennett, S.J., and J.L. Best (1995), Mean flow and turbulence structure over fixed, two-dimensional dunes: implications for sediment transport and bedform stability. *Sedimentology, 42,* 491–513.

Davies, A. G. (1977), A mathematical model of sediment in suspension in a uniform reversing tidal flow. Geophysical Journal of the Royal Astronomical Society, 51, 503-529. doi: 10.1111/j.1365-246X.1977.tb06932.x

Domarad, N. (2011), Flow and suspended sediment transport through the gravel-sand transition in the Fraser River, British Columbia. M.Sc. thesis, 110 pp., Dept. Geog., Simon Fraser Univ., Burnaby, British Columbia, Canada.

Gartner, J. W. (2004), Estimating suspended solids concentrations from backscatter intensity measured by acoustic Doppler current profiler in San Francisco Bay, California. *Mar. Geol., 211*, 169-187. doi: 10.1016/j.margeo.2004.07.001.

Geyer, W., and D. Farmer (1989), Tide-induced variation of the dynamics of a salt wedge estuary, *J. Phys. Oceanogr., 19*, 1060– 1672.

Gordon, C.M. (1975), Sediment entrainment and suspension in a tidal flow, *Mar. Geol., 18*, 57-64. doi: 10.1016/0025-3227(75)90040-7.

Jackson, R. G. (1976), Sedimentological and fluid-dynamic implications of the turbulence bursting phenomenon in geophysical flows, *J. Fluid Mech., 77*, 531–560.

Kim, H. T., S. J. Kline and W. C. Reynolds (1971), The production of turbulence near a smooth wall in a turbulent boundary layer, *J. Fluid Mech., 5* , 133-160, doi:10.1017/S0022112071002490

Kostaschuk, R. A. (2000), A field study of turbulence and sediment dynamics over subaqueous dunes with flow separation, *Sedimentology, 47*, 519– 531.

Kostaschuk, R. A. (2002), Flow and Sediment Dynamics in Migrating Salinity Intrusions: Fraser River Estuary Canada, *Estuaries, 25:(2),* 197-203.

Kostaschuk, R. A., and M. A. Church (1993), Macroturbulence generated by dunes: Fraser River, Canada, *Sediment. Geol., 85,* 25-37.

Kostaschuk, R. A., and P.V. Villard (1996), Flow and sediment transport over large subaqueous dunes: Fraser River, Canada, *Sedimentology, 43*, 849-863.

Kostaschuk, R. A., and P. V. Villard (1999), Turbulent sand suspension over dunes, in Fluvial Sedimentology VI, edited by N. D. Smith and J. Rogers, Spec. Publ. Int. Assoc. Sedimentol., 28, 3-14.

Kostaschuk, R., and J. Best (2005), Response of sand dunes to variations in tidal flow: Fraser Estuary, Canada, J. Geophys. Res., 110, F04S04, doi:10.1029/2004JF000176.

Kostaschuk, R. A., M. A. Church, and J.L. Luternauer (1989), Bed-material, bedforms and bed load in a salt-wedge estuary Fraser River, British Columbia, *Can. J. Earth Sci., 26,* 1440-1452.

Kostaschuk, R. A., P. V. Villard, and J. L. Best (2004), Measuring velocity and shear stress over dunes with an acoustic Doppler profiler, *J. Hydraul. Eng., 130*, 932–936.

Kostaschuk, R. A., J. L. Best, and P.V. Villard (2010), The influence of dunes on mixing in a migrating salt-wedge: Fraser River estuary, Canada, *Earth Surf. Process. Landforms, 35,* 460-465. doi: 10.1002/esp.1928.

Kostaschuk, R. A., J. L. Best, P. V. Villard, J. Peakall, and M. Franklin (2005), Measuring flow velocity and sediment transport with an acoustic Doppler current profiler, *Geomorphology, 65,* 25-37.

Levi, E. (1991), Vortices in hydraulics, *J. Hydraul. Eng., 117 (4)*, 399-413.

Lu, S. S., and W. W. Willmarth (1973), Measurements of the structure of the Reynolds stress in a turbulent boundary layer, *J. Fluid Mech., 60*, 481–511.

MacDonald, D., and A. Horner-Devine (2008), Temporal and spatial variability of vertical salt flux in a highly stratified estuary, *J. Geophys. Res., 113*, C09022, doi:10.1029/2007JC004620.

Mark, D. M. and M. A. Church (1977), On the misuse of regression in earth science, *Mathematical Geology*, *9*, 63-77. doi: 10.1007/BF02312496.

McLean, S. R., J. M. Nelson, and S.R. Wolfe (1994), Turbulence structure over two-dimensional bedforms: implications for sediment transport, *J. Geophys. Res., 99*, 12729-12747.

McLean, D. G., M. A. Church and B. Tassone (1999), Sediment transport along lower Fraser River. 1. Measurements and hydraulic computations, *Water Resour. Res., 35*, 2533-2548, doi: 10.1029/1999WR900101

Muller, A., and A. Gyr, (1986), On the vortex formation in the mixing layer behind dunes, *J. Hydraul. Res., 24*, 359–375.

Narahari Rao, K., R. Narasimha and M. A. Badri Narayanan (1971), The 'bursting' phenomenon in a turbulent boundary layer, *J. Fluid Mech., 48*, 339-352, doi:10.1017/S0022112071001605.

Nelson, J. M., S. R. McLean, and S.R. Wolfe (1993), Mean flow and turbulence fields over two-dimensional bedforms, *Water Resour. Res., 29,* 3935-3953.

Nelson, J. M., R. L. Shreve, S. R. McLean, and T. G. Drake (1995), Role of near-bed turbulence structure in bed load transport and bed form mechanics, *Water Resour. Res., 31*, 2071–2086.

Nezu, I., and H. Nakagawa (1993), Turbulence in Open-Channel Flows, 281 pp., A. A. Balkema, Brookfield, Vt.

Omidyeganeh, M, and U. Piomelli (2011), Large-eddy simulation of two dimensional dunes in a steady, unidirectional flow, *Journal of Turbulence*, *12*, N42.

Parsons, D. R., J. L. Best, O. Orfeo, R. J. Hardy, R. A. Kostaschuk, and S.N. Lane (2005), The morphology and flow fields of three-dimensional dunes, Rio Paraná, Argentina: results from simultaneous multibeam echo sounding and acoustic Doppler current profiling. *J. Geophys. Res,. 110*, F04S03, doi:10.1029/2004JF000231

Rennie, C. D., and F. Rainville (2006), Case study of precision of GPS differential correction strategies: Influence on aDcp velocity and discharge estimates, *J. Hydraul. Eng., 132*, 225‑234, doi:10.1061/(ASCE)0733-9429(2006)132:3(225).

Rennie, C. D., and M. A. Church (2010), Mapping spatial distributions and uncertainty of water and sediment flux in a large gravel bed river reach using an acoustic Doppler current profiler, *J. Geophys. Res.*, **115**, F03035, doi:10.1029/2009JF001556.

Rennie, C. D., R. G. Millar, and M. A. Church (2002), Measurement of bed load velocity using an acoustic Doppler current profiler, *J. Hydraul. Eng., 128*, 47-483, doi:10.1061/(ASCE)0733-9429(2002)128:5(473).

Rennie, C. D., F. Rainville, and S. Kashyap (2007), Improved estimation of ADCP apparent bed-load velocity using a real‐time Kalman filter, *J. Hydraul. Eng., 133*, 1337-1344, doi:10.1061/(ASCE)0733-9429(2007).

Reson Inc. (2009), SeaBat 7101 High-Resolution Multibeam Echosounder System, Operator's Manual, 168 pp, Denmark.

Roden, J. E. (1998), The sedimentology and dynamics of mega-dunes, Jamuna River, Bangladesh, Ph.D. thesis, 310 pp., Dep. of Earth Sci., Univ. of Leeds, Leeds, U. K.

Rood, K. M., and E. J. Hickin (1989), Suspended sediment concentration in relation to surface-flow structure in Squamish River estuary, southwestern British Columbia, *Can. J. Earth Sci., 26*, 2172–2176.

Schulkin, M., and H. W. Marsh (1962), Sound absorption in sea water, J*. Acoust. Soc. Am., 34(6)*, 864-865.

Shugar, D.H., R. A. Kostaschuk, J. L. Best, D. R. Parsons, S. N. Lane, O. Orfeo, and R. J. Hardy (2010), On the relationship between flow and suspended sediment transport over the crest of a sand dune, Río Paraná, Argentina, *Sedimentology*, *57,* 252-272, doi: 10.1111/j.1365-3091.2009.01110.x.

Smith, J.D., and S.R. McLean (1977), Spatially-averaged flow over a wavy surface, *J. Geophys. Res.*, *82*, 1735-1746.

Tedford, E. W., J. R. Carpenter, R. Pawlowicz, R. Pieters, and G. A. Lawrence (2009), observation and analysis of shear instability in the Fraser River estuary, *J. Geophys. Res., 114*, C11006, doi:10.1029/2009JC005313.

Teledyne RD Instruments (2001), WorkHorse Monitor ADCP User's Guide. 28 pp.

Topping, D. J., S. A. Wright, T.S. Melis, and D.M. Rubin (2007), High-resolution measurements of suspended-sediment concentration and grain size in the Colorado River in Grand Canyon using a multi-frequency acoustic system, in Proceedings of the 10th International Symposium on River Sedimentation, August 1–4, Moscow, Russia.

Villard, P.V and M. Church (2003), Dunes and associated sand transport in a tidally influence sand-bed channel: Fraser River, British Columbia, *Can. J. Earth Sci.*, *40*, 115-130.

Venditti, J.G. (in print), Bedforms in sand-bedded rivers, in *Treatise on Geomorphology*. Edited by Shroder, J., Jr., Wohl, E. Academic Press, San Diego, CA. 9**,** pp 26.

Venditti, J. G., and S. J. Bennett (2000), Spectral analysis of turbulent flow and suspended sediment transport over fixed dunes, *J. Geophys. Res., 105*, 22035–22047.

Venditti, J. G., and B. O. Bauer (2005), Turbulent flow over a dune: Green River, Colorado, *Earth Surf. Processes Landforms, 30,* 289–304, doi:10.1002/esp.1142.

Wright, S. A., D. J. Topping and C. A. Williams (2010), Discriminating Silt-and-clay from Suspended Sand in Rivers Using Side-Looking Acoustic Profilers, in 2nd Joint Federal Interagency Conference, July 24-June 1, Las Vegas, Nevada, USA.

Yalin, M. S. (1992), River Mechanics, 219 pp., Elsevier, New York.